Smart Mater. Struct. **18** (2009) 025009 (18pp) doi:10.1088/0964-1726/18/2/025009

An experimentally validated bimorph cantilever model for piezoelectric energy harvesting from base excitations

A Erturk[1,3] **and D J Inman**[2]

[1] Center for Intelligent Material Systems and Structures, Department of Engineering Science and Mechanics, Virginia Tech, Blacksburg, VA 24061, USA
[2] Center for Intelligent Material Systems and Structures, Department of Mechanical Engineering, Virginia Tech, Blacksburg, VA 24061, USA

E-mail: erturk@vt.edu

Received 28 May 2008, in final form 16 November 2008
Published 13 January 2009
Online at stacks.iop.org/SMS/18/025009

Abstract
Piezoelectric transduction has received great attention for vibration-to-electric energy conversion over the last five years. A typical piezoelectric energy harvester is a unimorph or a bimorph cantilever located on a vibrating host structure, to generate electrical energy from base excitations. Several authors have investigated modeling of cantilevered piezoelectric energy harvesters under base excitation. The existing mathematical modeling approaches range from elementary single-degree-of-freedom models to approximate distributed parameter solutions in the sense of Rayleigh–Ritz discretization as well as analytical solution attempts with certain simplifications. Recently, the authors have presented the closed-form analytical solution for a unimorph cantilever under base excitation based on the Euler–Bernoulli beam assumptions. In this paper, the analytical solution is applied to bimorph cantilever configurations with series and parallel connections of piezoceramic layers. The base excitation is assumed to be translation in the transverse direction with a superimposed small rotation. The closed-form steady state response expressions are obtained for harmonic excitations at arbitrary frequencies, which are then reduced to simple but accurate *single-mode* expressions for modal excitations. The electromechanical frequency response functions (FRFs) that relate the voltage output and vibration response to translational and rotational base accelerations are identified from the multi-mode and single-mode solutions. Experimental validation of the single-mode coupled voltage output and vibration response expressions is presented for a bimorph cantilever with a tip mass. It is observed that the closed-form single-mode FRFs obtained from the analytical solution can successfully predict the coupled system dynamics for a wide range of electrical load resistance. The performance of the bimorph device is analyzed extensively for the short circuit and open circuit resonance frequency excitations and the accuracy of the model is shown in all cases.

(Some figures in this article are in colour only in the electronic version)

1. Introduction

The drastic reduction in power requirements of small electronic components has motivated the research for powering such components by using the vibration energy available in their environment, especially in remote/wireless sensing applications. As proposed by Williams and Yates [1], the three basic vibration-to-electric energy conversion mechanisms are electromagnetic [1–3], electrostatic [4] and piezoelectric [5–7] transductions. In the past decade, these transduction mechanisms have been investigated by numerous researchers for vibration-based energy harvesting and extensive discussions

[3] Author to whom any correspondence should be addressed.

can be found in the existing review articles (e.g., Beeby *et al* [8]). The literature of the last five years shows that the piezoelectric transduction has received the greatest attention for vibration-to-electric energy conversion and three review articles specifically dealing with piezoelectric energy harvesting have been published in the past two years [5–7].

Typically, a piezoelectric energy harvester is a cantilevered beam with one or two piezoceramic layers (a unimorph or a bimorph). Basically, the harvester beam is located on a vibrating host structure and the dynamic strain induced in the piezoceramic layer(s) generates an alternating voltage output across the electrodes covering the piezoceramic layer(s). In addition to the experimental research on possible applications of such harvesters, researchers have proposed various mathematical models. Although the implementation of piezoelectric energy harvesting for charging a real battery in an efficient way is more sophisticated due to the AC-to-DC (alternating current-to-direct current) conversion process [9–13], researchers have considered a resistive electrical load in the circuit to come up with a simple model for predicting the electrical outputs for a given base motion input. The coupled problem of predicting the voltage across the resistive load connected to the electrodes of a vibrating harvester under base excitation has been investigated by many authors. The early modeling attempts of piezoelectric energy harvesters employed single-degree-of-freedom (SDOF) solutions [14, 15]. SDOF modeling (i.e., lumped parameter modeling) is a convenient modeling approach since the electrical domain already consists of lumped parameters: a capacitor (due to the internal capacitance of piezoceramic) and a resistor (due to an external load resistance). Hence, the only thing required is to obtain the lumped parameters representing the mechanical domain so that the mechanical equilibrium and electrical loop equations can be coupled through the piezoelectric constitutive relations [16]. This was the main procedure followed by Roundy *et al* [14] and duToit *et al* [15] in their SDOF model derivations. Although SDOF modeling gives initial insight into the problem by allowing simple expressions, it is an approximation limited to a single vibration mode and it lacks important aspects of the physical system, such as the dynamic mode shape and accurate strain distribution as well as their effects on the electrical response. Since cantilevered harvesters are excited due to the motion of their base, the well-known SDOF harmonic base excitation relation taken from the elementary vibration texts has been used in the energy harvesting literature both for modeling [15] and studying the optimization [17] of energy harvesters. It was recently shown [18] that the traditional form of the SDOF harmonic base excitation relation may yield highly inaccurate results both for the transverse and longitudinal vibrations of cantilevered harvesters depending on the tip (proof) mass to beam/bar mass ratio. Correction factors were derived [18] to improve the predictions of SDOF electromechanical relations [15] of cantilevered harvesters under base excitation.

As an improved modeling approach, the Rayleigh–Ritz type discrete formulation derived by Hagood *et al* [19] (based on the generalized Hamilton's principle for electromechanical systems due to Crandall *et al* [20]) was employed by Sodano *et al* [21] and duToit *et al* [15] for modeling of cantilevered piezoelectric energy harvesters (based on the Euler–Bernoulli beam theory). The Rayleigh–Ritz solution gives a discrete model of the distributed parameter system and it is a more accurate approximation compared to SDOF modeling. In order to represent the electrical outputs analytically, Lu *et al* [22] used the vibration mode shapes obtained from the Euler–Bernoulli beam theory and the piezoelectric constitutive relation [16] that gives the electric displacement to relate the electrical outputs to the mechanical mode shape. Similar models were given by Chen *et al* [23] and Lin *et al* [24] where the electrical response is expressed in terms of the beam vibration response. The issues in these analytical modeling attempts include not considering the resonance phenomenon and modal expansion as well as oversimplified modeling of piezoelectric coupling in the beam equation as viscous damping [22–24]. As shown in this work, representing the effect of piezoelectric coupling in the beam equation as viscous damping fails in predicting the coupled system dynamics of a *piezoelectric* energy harvester, although this approach works for certain *electromagnetic* energy harvesters [1]. In terms of analytical modeling, more recently, Ajitsaria *et al* [25] presented a bimorph cantilever model, where they attempted to combine the static sensing/actuation equations (with constant radius of curvature and a static tip force) with the dynamic Euler–Bernoulli beam equation (where the radius of curvature varies) under base excitation (where there is no tip force). Thus, highly different modeling approaches have appeared in the literature during the past five years and some of them might be misleading due to weak mathematical assumptions involved [26].

Recently, Erturk and Inman [27] have presented the analytical solution to the coupled problem of a unimorph piezoelectric energy harvester configuration based on the Euler–Bernoulli assumptions. They obtained the coupled voltage response across the resistive load and the coupled vibration response of the harvester explicitly for harmonic base excitations in the form of translation with small rotation. The short circuit and open circuit trends and the effect of piezoelectric coupling were investigated extensively [27]. Later, Elvin and Elvin [28] have observed the convergence of the Rayleigh–Ritz type of solution formerly introduced by Hagood *et al* [19] to the analytical solution given by Erturk and Inman [27] when sufficient number of vibration modes is used with appropriate admissible functions.

This paper presents the application of the coupled distributed parameter solution [27] to bimorph cantilever configurations with series and parallel connections of piezoceramic layers. The steady state voltage response and vibration response expressions are derived for harmonic excitation of the base at an arbitrary excitation frequency (in the form of translation in the transverse direction with small rotation). Then, by using the complete (multi-mode) solutions, the response expressions are reduced to simple but accurate *single-mode* relations. The single-mode relations can be used instead of the multi-mode relations for modal excitations (i.e., for excitations around resonance) of cantilevered bimorphs

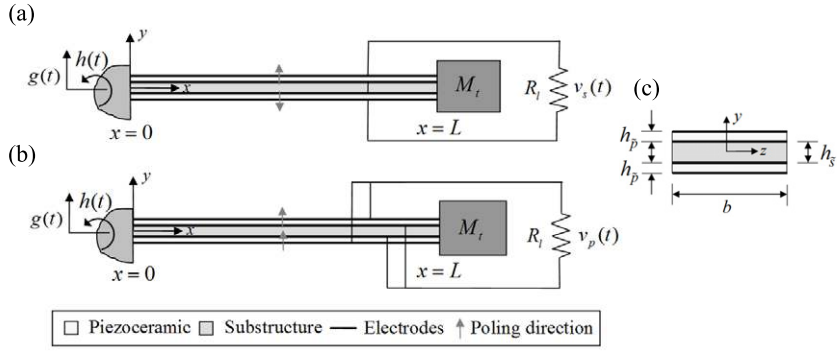

Figure 1. Bimorph cantilever configurations with (a) series connection of piezoceramic layers, (b) parallel connection of piezoceramic layers and the (c) cross-sectional view of a bimorph cantilever.

since the resonance excitation is the main concern in vibration-based energy harvesting. The electromechanical FRFs that give the voltage output and vibration response-to-translational and rotational base acceleration relations are extracted from the multi-mode and single-mode solutions. Experimental validation of the analytical formulation is given for a bimorph cantilever with a tip mass. It is shown that the single-mode analytical relations proposed here are very accurate in predicting the voltage output and vibration response FRFs. The bimorph device is analyzed extensively for the short circuit and open circuit resonance frequency excitations by using different resistive loads and it is observed that the analytical model can successfully predict the coupled system dynamics.

2. Fundamentals of the coupled distributed parameter model

This section reviews the assumptions in distributed parameter electromechanical modeling and introduces the two possible bimorph configurations based on the connection of the piezoceramic layers. Derivation of the coupled beam equation in physical coordinates is given along with the relevant expressions for the modal analysis. Derivation of the electrical circuit equation for an instantaneous deflection of a vibrating cantilever is explained based on the fundamentals of piezoelectricity and analytical structural dynamics.

2.1. Bimorph configurations and modeling assumptions

It is known from the literature of static sensing/actuation that, depending on the voltage or current requirements, the piezoceramic layers of a symmetric bimorph can be combined in series or in parallel (see, for instance, Wang and Cross [29]). This common practice of static sensing/actuation problems is valid for the dynamic piezoelectric energy harvesting problem as well. Each of the two bimorph configurations displayed in figures 1(a) and (b) undergoes bending vibrations due to the motion of its base. The piezoceramic layers are assumed to be identical and conductive electrodes are assumed to be fully covering the respective surfaces of these layers (top and bottom). The instantaneous bending strain in the top and bottom layers at an arbitrary position x over the beam length have the opposite sign (i.e., one is in tension whereas the other is in compression). As a consequence, since the piezoceramic layers of the bimorph shown in figure 1(a) are poled oppositely in the thickness direction (i.e., y-direction), this configuration represents the *series connection* of the piezoceramic layers. Likewise, figure 1(b) represents the *parallel connection* of the piezoceramic layers because the layers are poled in the same direction.

The bimorph cantilever configurations are modeled here as uniform composite beams based on the Euler–Bernoulli beam assumptions. Therefore, plane sections are assumed to remain plane during the vibratory motion and the effects of shear deformation and rotary inertia are neglected. This is a reasonable assumption since typical cantilevered energy harvesters are designed and manufactured as fairly thin beams. The mechanical losses are represented by internal and external damping mechanisms. The internal damping mechanism is assumed to be in the form of strain rate (or Kelvin–Voigt) damping and the effect of external (air) damping is considered with a separate damping coefficient. The piezoceramic and substructure layers are assumed to be perfectly bonded to each other. The electrodes covering the opposite faces of piezoceramic layers are assumed to be very thin when compared to the overall thicknesses of the harvester so that their contribution to the thickness dimension is negligible.

The continuous electrode pairs covering the top and the bottom faces of the piezoceramic layers are assumed to be perfectly conductive so that a single electric potential difference can be defined across them. Therefore, the instantaneous electric fields induced in the piezoceramic layers are assumed to be uniform throughout the length of the beam. A resistive electrical load (R_l) is considered in the circuit along with the internal capacitances of the piezoceramic layers. Note that, considering a resistive load in the electrical domain is a common practice in modeling of vibration-based energy harvesters [14, 15, 21–28]. As a consequence, it is assumed that the base motion input is persistent so that continuous electrical outputs can be extracted from the electromechanical system.

2.2. Coupled mechanical equation and modal analysis of a bimorph cantilever

As far as the mechanical aspect of the problem is concerned, the bimorph configurations shown in figures 1(a) and (b) are

identical. That is, they have the same geometric and material properties. However, the *backward* piezoelectric coupling effect in the beam equation due to piezoelectric constitutive relations is different for series and parallel connections of the piezoceramic layers, and expectedly, this affects the vibration response of the cantilever. In the following, the beam equations are derived for these two configurations and the analytical modal analysis relations are presented.

The motion of the base for each of the cantilevers shown in figures 1(a) and (b) is represented by translation $g(t)$ in the transverse direction with superimposed small rotation $h(t)$. Therefore, the effective base displacement $w_b(x,t)$ in the transverse direction can be written as [27]

$$w_b(x,t) = g(t) + xh(t). \tag{1}$$

The partial differential equation governing the forced vibrations of a uniform cantilevered bimorph (with a tip mass) under base excitation is

$$\frac{\partial^2 M(x,t)}{\partial x^2} + c_s I \frac{\partial^5 w_{rel}(x,t)}{\partial x^4\,\partial t} + c_a \frac{\partial w_{rel}(x,t)}{\partial t} + m\frac{\partial^2 w_{rel}(x,t)}{\partial t^2} = -[m + M_t\delta(x-L)]\frac{\partial^2 w_b(x,t)}{\partial t^2} \tag{2}$$

where $w_{rel}(x,t)$ is the transverse deflection of the beam relative to its base at position x and time t, $M(x,t)$ is the internal bending moment (excluding the strain rate damping effect), $c_s I$ is the equivalent damping term of the composite cross-section due to strain rate damping (c_s is the equivalent coefficient of strain rate damping and I is the equivalent area moment of inertia of the composite cross-section), c_a is the viscous air damping coefficient, m is the mass per unit length of the beam, M_t it is tip mass and $\delta(x)$ is the Dirac delta function. Both of the damping mechanisms are assumed to satisfy the proportional damping criterion, hence, they are mathematically convenient for the modal analysis solution procedure[4]. Note that the effect of strain rate damping is an internal bending moment and it is directly written outside the term $M(x,t)$ in equation (2).

Instead of defining the damping coefficients in the physical equation of motion, one could consider the corresponding undamped equation (by setting $c_s I = c_a = 0$ in equation (2)) and introduce modal damping to the equation of motion in modal coordinates as is common practice. It is worthwhile to mention that the foregoing consideration of the mechanical damping components results in an additional excitation term due to external damping as shown in Erturk and Inman [18]. Typically, for harvesters operating in air, the external damping excitation is negligible when compared to the inertial excitation term. It was shown in a dimensionless basis that, in the absence of a tip mass, the amount of modal forcing due to external damping term is less than 5% of the total modal base excitation force if the component of the modal damping ratio due to external damping is less than 2.5% (see figure 3 in [18]). Therefore the damping excitation term is directly omitted in equation (2) for simplicity. However, excitation due to external damping can be important for harvesters operating in fluids with larger damping effect and the general form of the forcing function must be used in that case [18, 27].

The internal bending moment term in equation (2) is the first moment of axial strain over the cross-section:

$$M(x,t) = -b\left(\int_{-h_{\tilde{p}}-h_{\tilde{s}}/2}^{-h_{\tilde{s}}/2} T_1^{\tilde{p}} y\,dy + \int_{-h_{\tilde{s}}/2}^{h_{\tilde{s}}/2} T_1^{\tilde{s}} y\,dy + \int_{h_{\tilde{s}}/2}^{h_{\tilde{p}}+h_{\tilde{s}}/2} T_1^{\tilde{p}} y\,dy\right) \tag{3}$$

where b is the width, $h_{\tilde{p}}$ is the thickness of each piezoceramic layer and $h_{\tilde{s}}$ is the thickness of the substructure layer (figure 1(c)). Furthermore, $T_1^{\tilde{p}}$ and $T_1^{\tilde{s}}$ are the axial stress components in the piezoceramic and substructure layers, respectively (1-direction is the longitudinal direction, i.e., x-direction), and they are given by the following constitutive relations:

$$T_1^{\tilde{s}} = Y_{\tilde{s}} S_1^{\tilde{s}}, \qquad T_1^{\tilde{p}} = \bar{c}_{11}^E S_1^{\tilde{p}} - \bar{e}_{31} E_3 \tag{4}$$

where $Y_{\tilde{s}}$ is Young's modulus of the substructure layer, $\bar{c}_{11}^E$ is the elastic stiffness (i.e., Young's modulus) of the piezoceramic layer at constant electric field, $\bar{e}_{31}$ is the piezoelectric constant and E_3 is the electric field component in 3-direction (i.e., y-direction). Here and hereafter, the subscripts and superscripts $\tilde{p}$ and $\tilde{s}$ stand for the piezoceramic and the substructure layers, respectively. Based on the plane-stress assumption for a beam, the elastic stiffness component can be expressed as $\bar{c}_{11}^E = 1/s_{11}^E$, where s_{11}^E is the elastic compliance at constant electric field. Furthermore, based on the same assumption, $\bar{e}_{31}$ can be given in terms of the more commonly used piezoelectric constant d_{31} as $\bar{e}_{31} = d_{31}/s_{11}^E$. The axial strain components in the piezoelectric and substructure layers are given by $S_1^{\tilde{p}}$ and $S_1^{\tilde{s}}$, respectively, and they are due to bending only. Hence the axial strain at a certain level (y) from the neutral axis of the composite beam is simply proportional to the curvature of the beam at that position (x):

$$S_1(x,y,t) = -y\frac{\partial^2 w_{rel}(x,t)}{\partial x^2}. \tag{5}$$

The electric field component E_3 should be expressed in terms of the respective voltage term in each bimorph configuration (figures 1(a) and (b)). This is the point where the resulting mechanical equations for series and parallel connections of the piezoceramic layers differ from each other. Since the piezoceramic layers are assumed to be identical, voltage across the electrodes of each piezoceramic layer is $v_s(t)/2$ in the series connection case (figure 1(a)). Expectedly, for the parallel connection case (figure 1(b)), voltage across the electrodes of each piezoceramic layer is $v_p(t)$. It is worthwhile to add that $\bar{e}_{31}$ has the opposite sign for the top and the bottom piezoceramic layers for the series connection case (due to opposite poling) so that the instantaneous electric fields are in the same direction (i.e., $E_3(t) = -v_s(t)/2h_{\tilde{p}}$ in both layers). For the configuration with parallel connection, since $\bar{e}_{31}$ has the same sign in top and bottom piezoceramic layers,

[4] Strain rate damping is assumed to be stiffness proportional whereas air damping is assumed to be mass proportional and this type of damping is also known as the Rayleigh damping [30]. Modeling and identification of more sophisticated damping mechanisms in beams were investigated by Banks and Inman [31].

the instantaneous electric fields are in the opposite directions (i.e., $E_3(t) = -v_p(t)/h_{\tilde{p}}$ in the top layer and $E_3(t) = v_p(t)/h_{\tilde{p}}$ in the bottom layer). Another important point is that, for both configurations, the piezoelectric coupling term coming from equation (3) is a function of time only. Hence, before substituting equation (3) into (2), the electrical term must be multiplied by $[H(x) - H(x-L)]$, where $H(x)$ is the Heaviside function. Since the voltage outputs of the series and parallel connection cases are different, the piezoelectric coupling effect in the mechanical equation (equation (2)) is expected to be different. Thus, in the rest of the paper, the mechanical response expressions of the series and parallel connection configurations are denoted by $w^{s}_{rel}(x,t)$ and $w^{p}_{rel}(x,t)$, respectively. Note that, here and hereafter, the subscripts and superscripts s and p stand for *series* and *parallel* connections of the piezoceramic layers.

Based on the foregoing discussion, the coupled beam equation can be obtained for the series connection case (figure 1(a)) as follows:

$$\begin{aligned} &YI\frac{\partial^4 w^{s}_{rel}(x,t)}{\partial x^4} + c_s I\frac{\partial^5 w^{s}_{rel}(x,t)}{\partial x^4 \partial t} + c_a\frac{\partial w^{s}_{rel}(x,t)}{\partial t} \\ &\quad + m\frac{\partial^2 w^{s}_{rel}(x,t)}{\partial t^2} + \vartheta_s v_s(t)\left[\frac{d\delta(x)}{dx} - \frac{d\delta(x-L)}{dx}\right] \\ &= -[m + M_t\delta(x-L)]\frac{\partial^2 w_b(x,t)}{\partial t^2} \end{aligned} \tag{6}$$

where the piezoelectric coupling term ϑ_s for the series connection case is

$$\vartheta_s = \frac{\bar{e}_{31} b}{2h_{\tilde{p}}}\left[\frac{h_{\tilde{s}}^2}{4} - \left(h_{\tilde{p}} + \frac{h_{\tilde{s}}}{2}\right)^2\right]. \tag{7}$$

Similarly, one can obtain the equation of motion for the case with the parallel connection of the piezoceramic layers as (figure 1(b))

$$\begin{aligned} &YI\frac{\partial^4 w^{p}_{rel}(x,t)}{\partial x^4} + c_s I\frac{\partial^5 w^{p}_{rel}(x,t)}{\partial x^4 \partial t} + c_a\frac{\partial w^{p}_{rel}(x,t)}{\partial t} \\ &\quad + m\frac{\partial^2 w^{p}_{rel}(x,t)}{\partial t^2} + \vartheta_p v_p(t)\left[\frac{d\delta(x)}{dx} - \frac{d\delta(x-L)}{dx}\right] \\ &= -[m + M_t\delta(x-L)]\frac{\partial^2 w_b(x,t)}{\partial t^2} \end{aligned} \tag{8}$$

where the backward coupling term ϑ_p for the parallel connection case can be expressed as

$$\vartheta_p = 2\vartheta_s = \frac{\bar{e}_{31} b}{h_{\tilde{p}}}\left[\frac{h_{\tilde{s}}^2}{4} - \left(h_{\tilde{p}} + \frac{h_{\tilde{s}}}{2}\right)^2\right]. \tag{9}$$

In equations (6) and (8), the bending stiffness term YI and the mass per unit length term m are simply

$$\begin{aligned} YI &= \frac{2b}{3}\left[Y_{\tilde{s}}\frac{h_{\tilde{s}}^3}{8} + \bar{c}_{11}^{E}\left(\left(h_{\tilde{p}} + \frac{h_{\tilde{s}}}{2}\right)^3 - \frac{h_{\tilde{s}}^3}{8}\right)\right], \\ m &= b(\rho_{\tilde{s}} h_{\tilde{s}} + 2\rho_{\tilde{p}} h_{\tilde{p}}) \end{aligned} \tag{10}$$

where $\rho_{\tilde{s}}$ and $\rho_{\tilde{p}}$ are the mass densities of the substructure and the piezoceramic materials, respectively.

Based on the proportional damping assumption, the vibration response relative to the base of the bimorph (figures 1(a) and (b)) can be represented as an absolutely and uniformly convergent series of the eigenfunctions as

$$w^{s}_{rel}(x,t) = \sum_{r=1}^{\infty}\phi_r(x)\eta_r^{s}(t), \tag{11a}$$

$$w^{p}_{rel}(x,t) = \sum_{r=1}^{\infty}\phi_r(x)\eta_r^{p}(t) \tag{11b}$$

where $\phi_r(x)$ is the mass normalized eigenfunction of the rth vibration mode, $\eta_r^{s}(t)$ and $\eta_r^{p}(t)$ are the modal mechanical response expressions of the series and parallel connection cases, respectively. The eigenfunctions denoted by $\phi_r(x)$ are the mass normalized eigenfunctions of the corresponding undamped free vibration problem:

$$\phi_r(x) = C_r\left[\cos\frac{\lambda_r}{L}x - \cosh\frac{\lambda_r}{L}x + \varsigma_r\left(\sin\frac{\lambda_r}{L}x - \sinh\frac{\lambda_r}{L}x\right)\right] \tag{12}$$

where ς_r is obtained from

$$\varsigma_r = \frac{\sin\lambda_r - \sinh\lambda_r + \lambda_r\frac{M_t}{mL}(\cos\lambda_r - \cosh\lambda_r)}{\cos\lambda_r + \cosh\lambda_r - \lambda_r\frac{M_t}{mL}(\sin\lambda_r - \sinh\lambda_r)} \tag{13}$$

and C_r is a modal amplitude constant which should be evaluated by normalizing the eigenfunctions according to the following orthogonality conditions:

$$\begin{aligned} &\int_0^L \phi_s(x) m \phi_r(x)\,dx + \phi_s(L) M_t \phi_r(L) \\ &\quad + \left[\frac{d\phi_s(x)}{dx} I_t \frac{d\phi_r(x)}{dx}\right]_{x=L} = \delta_{rs} \\ &\int_0^L \phi_s(x) YI \frac{d^4\phi_r(x)}{dx^4}dx - \left[\phi_s(x) YI \frac{d^3\phi_r(x)}{dx^3}\right]_{x=L} \\ &\quad + \left[\frac{d\phi_s(x)}{dx} YI \frac{d^2\phi_r(x)}{dx^2}\right]_{x=L} = \omega_r^2\delta_{rs}. \end{aligned} \tag{14}$$

Here, I_t is the rotary inertia of the tip mass M_t and δ_{rs} is Kronecker delta, defined as being equal to unity for $s = r$ and equal to zero for $s \neq r$. Furthermore, ω_r is the undamped natural frequency of the rth vibration mode in short circuit conditions (i.e., as $R_l \to 0$) given by

$$\omega_r = \lambda_r^2\sqrt{\frac{YI}{mL^4}} \tag{15}$$

where the eigenvalues of the system (λ_r for mode r) are obtained from

$$\begin{aligned} &1 + \cos\lambda\cosh\lambda + \lambda\frac{M_t}{mL}(\cos\lambda\sinh\lambda - \sin\lambda\cosh\lambda) \\ &\quad - \frac{\lambda^3 I_t}{mL^3}(\cosh\lambda\sin\lambda + \sinh\lambda\cos\lambda) \\ &\quad + \frac{\lambda^4 M_t I_t}{m^2 L^4}(1 - \cos\lambda\cosh\lambda) = 0. \end{aligned} \tag{16}$$

It should be mentioned that the foregoing modal analysis is given for the short circuit conditions (i.e., for $R_l \to 0$) so

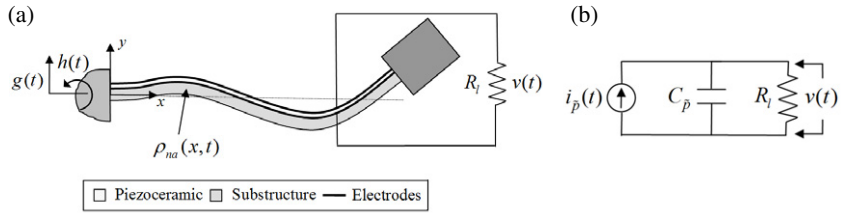

Figure 2. (a) Cantilever beam with a single piezoceramic layer under transverse vibrations (exaggerated view) and the (b) corresponding electrical circuit for a resistive electrical load connected to the electrodes.

that the conventional form of the eigenfunctions is obtained in equation (12) (since, for short circuit conditions, $v_s(t) \to 0$ and $v_p(t) \to 0$ in equations (6) and (8), respectively). Thus, for a given bimorph, the form of the eigenfunctions given by $\phi_r(x)$ and their mass normalization conditions are the same regardless of the series or parallel connections of the piezoceramic layers. For non-zero values of load resistance, the voltage terms in the mechanical equations take finite values, generating point moment excitations at the boundaries of the piezoceramic layer according to equations (6) and (8), and yielding two different modal mechanical response functions for these equations as $\eta_r^s(t)$ and $\eta_r^p(t)$, respectively (as obtained in sections 3.3 and 4.3). Therefore, the feedback from the voltage response for a given load resistance alters the mechanical response as well as the resonance frequency of the harvester, which are observed experimentally and predicted theoretically in section 7. At this stage, it should be underlined that the harvester beam has the resonance characteristics of the corresponding uncoupled (or *passive*) beam for $R_l \to 0$ only.

2.3. Coupled electrical circuit equation of a piezoceramic layer under dynamic bending

In order to derive the governing circuit equations of the bimorph configurations for series and parallel connections of the piezoceramic layers, one should first examine the electrical dynamics of a single layer under bending vibrations. Figure 2(a) displays a cantilevered beam with a single piezoceramic layer, i.e., a unimorph cantilever. Note that the deflections are exaggerated to highlight the space- and time-dependent radius of curvature of the neutral axis at an arbitrary point. The electrodes bracketing the piezoceramic layers fully cover the top and the bottom surfaces and they are connected to a resistive electrical load.

Since the only source of mechanical strain is assumed to be the axial strain due to bending, the tensorial representation of the relevant piezoelectric constitutive relation [16] that gives the vector of electric displacements can be reduced to the following scalar equation:

$$D_3 = \bar{e}_{31} S_1^{\tilde{p}} + \bar{\varepsilon}_{33}^S E_3 \tag{17}$$

where D_3 is the electric displacement component and $\bar{\varepsilon}_{33}^S$ is the permittivity component at constant strain with the plane-stress assumption ($\bar{\varepsilon}_{33}^S = \varepsilon_{33}^T - d_{31}^2/s_{11}^E$ where ε_{33}^T is the permittivity component at constant stress). Since the circuit admittance across the electrodes is $1/R_l$, the electric current output can be obtained from the Gauss law as [16]

$$\frac{\mathrm{d}}{\mathrm{d}t}\left(\int_A \mathbf{D}\cdot\mathbf{n}\,\mathrm{d}A\right) = \frac{v(t)}{R_l} \tag{18}$$

where $\mathbf{D}$ is the vector of electric displacement components in the piezoceramic layer, $\mathbf{n}$ is the unit outward normal and the integration is performed over the electrode area A [16, 27]. As can be anticipated, the only contribution to the inner product of the integrand in equation (18) is from D_3, since the electrodes are perpendicular to 3-direction (i.e., y-direction). After expressing the average bending strain in the piezoceramic layer in terms of the curvature (see equation (5)) and the uniform electric field in terms of the electric potential difference ($E_3(t) = -v(t)/h_{\tilde{p}}$), equation (17) can be used in equation (18) to obtain

$$\frac{\bar{\varepsilon}_{33}^S bL}{h_{\tilde{p}}}\frac{\mathrm{d}v(t)}{\mathrm{d}t} + \frac{v(t)}{R_l} = -\bar{e}_{31} h_{\tilde{p}c} b \int_0^L \frac{\partial^3 w_{\mathrm{rel}}(x,t)}{\partial x^2 \partial t}\mathrm{d}x \tag{19}$$

where b, $h_{\tilde{p}}$ and L are the width, thickness and the length of the piezoceramic layer, respectively, and $h_{\tilde{p}c}$ is the distance between the neutral axis and the center of the piezoceramic layer [27]. One can then substitute the modal expansion form given by

$$w_{\mathrm{rel}}(x,t) = \sum_{r=1}^{\infty} \phi_r(x)\eta_r(t) \tag{20}$$

in equation (19) to obtain

$$\frac{\bar{\varepsilon}_{33}^S bL}{h_{\tilde{p}}}\frac{\mathrm{d}v(t)}{\mathrm{d}t} + \frac{v(t)}{R_l} = \sum_{r=1}^{\infty} \kappa_r \frac{\mathrm{d}\eta_r(t)}{\mathrm{d}t} \tag{21}$$

where κ_r is the modal coupling term in the electrical circuit equation:

$$\kappa_r = -\bar{e}_{31} h_{\tilde{p}c} b \int_0^L \frac{\mathrm{d}^2\phi_r(x)}{\mathrm{d}x^2}\mathrm{d}x = -\bar{e}_{31} h_{\tilde{p}c} b \left.\frac{\mathrm{d}\phi_r(x)}{\mathrm{d}x}\right|_{x=L}. \tag{22}$$

The forward coupling term κ_r has important consequences as discussed by Erturk *et al* [27, 32] extensively. According to equation (19), which originates from the Gauss law given by equation (18), the excitation of the simple *RC* circuit considered here as well as that of more sophisticated harvesting circuit topologies [9–13] is proportional to the integral of the dynamic strain distribution over the electrode area. For vibration modes of a cantilevered beam other than

the fundamental (first) mode, the dynamic strain distribution over the beam length changes sign at the *strain nodes*. It is known from equation (5) that the curvature at a point is a direct measure of the bending strain. Hence, for modal excitations, strain nodes are the *inflection points* of the eigenfunctions and the integrand in equation (22) is the curvature eigenfunction. If the electric charge developed at the opposite sides of a strain node is collected by continuous electrodes for vibrations with a certain mode shape, cancelation occurs due to the phase difference in the mechanical strain distribution. Mathematically, the partial areas under the integrand function of the integral in equation (22) cancel each other over the domain of integration. As an undesired consequence, the excitation of the electrical circuit, and therefore the electrical outputs may diminish drastically. In order to avoid cancellations, segmented electrodes can be used in harvesting energy from the modes higher than the fundamental mode. The leads of the segmented electrodes can be combined in the circuit in an appropriate manner [32]. Note that the rth vibration mode of a clamped-free beam has $r-1$ strain nodes, and consequently, the first mode of a cantilevered beam has no cancelation problem. Some boundary conditions are more prone to strong cancellations. For instance, a beam with clamped–clamped boundary conditions has $r+1$ strain nodes for the rth vibration mode.

Based on equation (21), it is very useful to represent the electrical domain of the coupled system by the simple circuit shown in figure 2(b). It is known in the circuitry-based energy harvesting literature that a piezoelectric element can be represented as a current source in parallel with its internal capacitance [9, 10]. Therefore, the simple circuit shown in figure 2(b) is the complete circuit of the electrical domain for a single resistive load case. Note that, this representation considers the electrical domain *only* and the electromechanical representation of the coupled system is actually a *transformer* because of the voltage feedback sent to the mechanical domain due to piezoelectric coupling (which will be incorporated in the formulation here). The components of the circuit are the internal capacitance $C_{\tilde{p}}$ of the piezoceramic layer, the resistive load R_l and the current source $i_{\tilde{p}}(t)$. In agreement with figure 2(a), the voltage across the resistive load is denoted by $v(t)$. Then, the Kirchhoff laws can be applied to the electrical circuit shown in figure 2(b) to obtain

$$C_{\tilde{p}}\frac{\mathrm{d}v(t)}{\mathrm{d}t}+\frac{v(t)}{R_l}=i_{\tilde{p}}(t) \tag{23}$$

where the internal capacitance and the current source terms can be extracted by matching equations (21) and (23) as

$$C_{\tilde{p}}=\frac{\bar{\varepsilon}_{33}^{S}bL}{h_{\tilde{p}}},\qquad i_{\tilde{p}}(t)=\sum_{r=1}^{\infty}\kappa_r\frac{\mathrm{d}\eta_r(t)}{\mathrm{d}t}. \tag{24}$$

Identification of the above terms (especially the current source term) has a very practical use for modeling of multi-morph harvesters. This way, for a given number of piezoceramic layers, there is no need to derive the electrical circuit equation by using the constitutive relation and the Gauss law given by equations (17) and (18), respectively. Each piezoceramic layer will have a similar capacitance and current source term and the layers can be combined to the resistive electrical load(s) in a desired way. Here, however, we limit our discussion to bimorphs (two piezoceramic layers only) as presented in the following.

3. Bimorph cantilever model for series connection of the piezoceramic layers

Based on the fundamentals given in section 2, this section presents the derivation of the closed-form expressions for the coupled voltage response $v_s(t)$ and vibration response $w_{\mathrm{rel}}^{s}(x,t)$ of the bimorph configuration shown in figure 1(a). First the coupled mechanical equation is given in modal coordinates and then the coupled circuit equation is derived. The resulting coupled equations are then solved for the steady state voltage response and vibration response for harmonic base motion inputs.

3.1. Coupled beam equation in modal coordinates

After substituting equation (11*a*) into (6) and applying the orthogonality conditions given by equation (14), the mechanical equation of motion in modal coordinates can be obtained as

$$\frac{\mathrm{d}^2\eta_r^s(t)}{\mathrm{d}t^2}+2\zeta_r\omega_r\frac{\mathrm{d}\eta_r^s(t)}{\mathrm{d}t}+\omega_r^2\eta_r^s(t)+\chi_r^s v_s(t)=f_r(t) \tag{25}$$

where the modal electromechanical coupling term is

$$\chi_r^s=\vartheta_s\frac{\mathrm{d}\phi_r(x)}{\mathrm{d}x}\bigg|_{x=L} \tag{26}$$

and the modal mechanical forcing function can be expressed as

$$f_r(t)=-m\left(\frac{\mathrm{d}^2g(t)}{\mathrm{d}t^2}\int_0^L\phi_r(x)\,\mathrm{d}x+\frac{\mathrm{d}^2h(t)}{\mathrm{d}t^2}\int_0^L x\phi_r(x)\,\mathrm{d}x\right)-M_t\phi_r(L)\left(\frac{\mathrm{d}^2g(t)}{\mathrm{d}t^2}+L\frac{\mathrm{d}^2h(t)}{\mathrm{d}t^2}\right). \tag{27}$$

In equation (25), ζ_r is the modal mechanical damping ratio that includes the combined effects of strain rate and air damping. In the absence of a tip mass, how to relate the modal damping ratio to the strain rate and air damping terms c_sI and c_a mathematically based on the assumption of proportional damping can be found in the literature [18]. However, as a common experimental modal analysis practice, one can identify the modal damping ratio ζ_r of a desired mode directly from the frequency response or time domain measurements. In this way, the requirement of defining and obtaining the physical damping terms c_sI and c_a is avoided [27].

3.2. Coupled electrical circuit equation

As described in section 2.1, the piezoceramic layers of the bimorph configuration shown in figure 1(a) are connected in series. We know from the practice given in section 2.3 that each piezoceramic layer can be represented as a current source in parallel with its internal capacitance. Therefore, figure 3

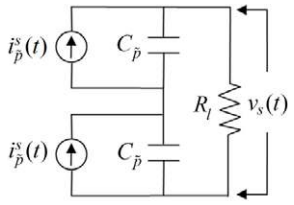

Figure 3. Electrical circuit representing the series connection of the piezoceramic layers.

displays the series connection of the identical piezoceramic layers of the bimorph configuration shown in figure 1(a).

Kirchhoff laws can be applied to the circuit depicted in figure 3 to obtain

$$\frac{C_{\tilde{p}}}{2}\frac{\mathrm{d}v_{\mathrm{s}}(t)}{\mathrm{d}t} + \frac{v_{\mathrm{s}}(t)}{R_{\mathrm{l}}} = i_{\tilde{p}}^{s}(t) \tag{28}$$

where the internal capacitance and the current source terms of the bimorph (for each layer) are

$$C_{\tilde{p}} = \frac{\bar{\varepsilon}_{33}^{S} bL}{h_{\tilde{p}}}, \qquad i_{\tilde{p}}^{s}(t) = \sum_{r=1}^{\infty} \kappa_r \frac{\mathrm{d}\eta_r^{\mathrm{s}}(t)}{\mathrm{d}t}. \tag{29}$$

The modal coupling term is then

$$\begin{aligned}\kappa_r &= -\bar{e}_{31} h_{\tilde{p}c} b \int_0^L \frac{\mathrm{d}^2\phi_r(x)}{\mathrm{d}x^2}\,\mathrm{d}x \\ &= -\frac{\bar{e}_{31}(h_{\tilde{p}} + h_{\tilde{s}})b}{2}\frac{\mathrm{d}\phi_r(x)}{\mathrm{d}x}\bigg|_{x=L}\end{aligned} \tag{30}$$

where $h_{\tilde{p}c}$ (the distance between the neutral axis and the center of the piezoceramic layer) is expressed in terms of the piezoceramic and the substructure layer thicknesses $h_{\tilde{p}}$ and $h_{\tilde{s}}$ (figure 1(c)). Hence, equation (28) is the electrical circuit equation of the bimorph cantilever for series connection of the piezoceramic layers.

3.3. Closed-form voltage response and vibration response expressions

Equations (25) and (28) constitute the coupled equations for the modal mechanical response $\eta_r^{\mathrm{s}}(t)$ of the bimorph and the voltage response $v_{\mathrm{s}}(t)$ across the resistive load. In this section, we derive the steady state solution of these terms for harmonic motion inputs. If the translational and rotational components of the base displacement given by equation (1) are harmonic of the forms $g(t) = Y_0 \mathrm{e}^{\mathrm{j}\omega t}$ and $h(t) = \theta_0 \mathrm{e}^{\mathrm{j}\omega t}$, where Y_0 and θ_0 are the translational and small rotational displacement amplitudes of the base, ω is the frequency and j is the unit imaginary number, then the modal forcing function given by equation (27) can be expressed as $f_r(t) = F_r \mathrm{e}^{\mathrm{j}\omega t}$ where the amplitude F_r is

$$\begin{aligned}F_r = \omega^2\Bigg[m\left(Y_0\int_0^L \phi_r(x)\mathrm{d}x + \theta_0\int_0^L x\phi_r(x)\mathrm{d}x\right) \\ + M_{\mathrm{t}}\phi_r(L)(Y_0 + L\theta_0)\Bigg].\end{aligned} \tag{31}$$

For the harmonic base motions at frequency ω, the steady state modal mechanical response of the beam and the steady state voltage response across the resistive load are assumed to be harmonic at the same frequency as $\eta_r^{\mathrm{s}}(t) = H_r^s \mathrm{e}^{\mathrm{j}\omega t}$ and $v_{\mathrm{s}}(t) = V_{\mathrm{s}} \mathrm{e}^{\mathrm{j}\omega t}$ (linear system assumption), respectively, where the amplitudes H_r^s and V_{s} are complex valued. Therefore, equations (25) and (28) yield the following two equations for H_r^s and V_{s}:

$$(\omega_r^2 - \omega^2 + \mathrm{j}2\zeta_r\omega_r\omega)H_r^s + \chi_r^s V_{\mathrm{s}} = F_r \tag{32}$$

$$\left(\frac{1}{R_{\mathrm{l}}} + \mathrm{j}\omega\frac{C_{\tilde{p}}}{2}\right)V_{\mathrm{s}} - \mathrm{j}\omega\sum_{r=1}^{\infty}\kappa_r H_r^s = 0. \tag{33}$$

The complex modal mechanical response amplitude H_r^s can be extracted from equation (32) and it can be substituted in equation (33) to obtain the complex voltage amplitude V_{s} explicitly. The resulting complex voltage amplitude can then be used in $v_{\mathrm{s}}(t) = V_{\mathrm{s}}\mathrm{e}^{\mathrm{j}\omega t}$ to express the steady state voltage response as

$$v_{\mathrm{s}}(t) = \frac{\sum_{r=1}^{\infty}\frac{\mathrm{j}\omega\kappa_r F_r}{\omega_r^2-\omega^2+\mathrm{j}2\zeta_r\omega_r\omega}}{\frac{1}{R_{\mathrm{l}}} + \mathrm{j}\omega\frac{C_{\tilde{p}}}{2} + \sum_{r=1}^{\infty}\frac{\mathrm{j}\omega\kappa_r\chi_r^s}{\omega_r^2-\omega^2+\mathrm{j}2\zeta_r\omega_r\omega}}\mathrm{e}^{\mathrm{j}\omega t}. \tag{34}$$

The complex voltage amplitude V_{s} can be substituted into equation (32) to obtain the steady state modal mechanical response of the bimorph as

$$\begin{aligned}\eta_r^{\mathrm{s}}(t) = &\left(F_r - \chi_r^s\frac{\sum_{r=1}^{\infty}\frac{\mathrm{j}\omega\kappa_r F_r}{\omega_r^2-\omega^2+\mathrm{j}2\zeta_r\omega_r\omega}}{\frac{1}{R_{\mathrm{l}}} + \mathrm{j}\omega\frac{C_{\tilde{p}}}{2} + \sum_{r=1}^{\infty}\frac{\mathrm{j}\omega\kappa_r\chi_r^s}{\omega_r^2-\omega^2+\mathrm{j}2\zeta_r\omega_r\omega}}\right) \\ &\times\frac{\mathrm{e}^{\mathrm{j}\omega t}}{\omega_r^2 - \omega^2 + \mathrm{j}2\zeta_r\omega_r\omega}.\end{aligned} \tag{35}$$

The transverse displacement response (relative to the base) at point x on the bimorph can be obtained in physical coordinates by substituting equation (35) in equation (11*a*):

$$\begin{aligned}&w_{\mathrm{rel}}^{\mathrm{s}}(x,t) \\ &= \sum_{r=1}^{\infty}\Bigg[\left(F_r - \chi_r^s\frac{\sum_{r=1}^{\infty}\frac{\mathrm{j}\omega\kappa_r F_r}{\omega_r^2-\omega^2+\mathrm{j}2\zeta_r\omega_r\omega}}{\frac{1}{R_{\mathrm{l}}} + \mathrm{j}\omega\frac{C_{\tilde{p}}}{2} + \sum_{r=1}^{\infty}\frac{\mathrm{j}\omega\kappa_r\chi_r^s}{\omega_r^2-\omega^2+\mathrm{j}2\zeta_r\omega_r\omega}}\right) \\ &\quad\times\frac{\phi_r(x)\mathrm{e}^{\mathrm{j}\omega t}}{\omega_r^2 - \omega^2 + \mathrm{j}2\zeta_r\omega_r\omega}\Bigg].\end{aligned} \tag{36}$$

Note that the vibration response given by equation (36) is the response of the beam relative to its moving base. If one is interested in the coupled beam displacement in the absolute physical coordinates (relative to the fixed frame), it is the superposition of the base displacement and the vibratory displacement relative to base:

$$w^{\mathrm{s}}(x,t) = w_{\mathrm{b}}(x,t) + w_{\mathrm{rel}}^{\mathrm{s}}(x,t) \tag{37}$$

where $w_{\mathrm{b}}(x,t)$ is the base displacement given by equation (1).

4. Bimorph cantilever model for parallel connection of the piezoceramic layers

This section aims to derive the steady state expressions for voltage response $v_{\mathrm{p}}(t)$ and the vibration response $w_{\mathrm{rel}}^{\mathrm{p}}(x,t)$ of the bimorph configuration shown in figure 1(b) to harmonic base motions. The coupled beam equation in modal coordinates and the electrical circuit equations are derived and the closed-form solutions are obtained in the following.

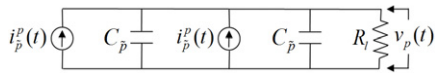

Figure 4. Electrical circuit representing the parallel connection of the piezoceramic layers.

4.1. Coupled beam equation in modal coordinates

After substituting equation (11*b*) in equation (8), the partial differential equation given by equation (8) can be reduced to an infinite set of ordinary differential equations in modal coordinates as follows:

$$\frac{\mathrm{d}^2\eta_r^{\mathrm{p}}(t)}{\mathrm{d}t^2} + 2\zeta_r\omega_r\frac{\mathrm{d}\eta_r^{\mathrm{p}}(t)}{\mathrm{d}t} + \omega_r^2\eta_r^{\mathrm{p}}(t) + \chi_r^p v_{\mathrm{p}}(t) = f_r(t) \quad (38)$$

where the modal electromechanical coupling term is

$$\chi_r^p = \vartheta_{\mathrm{p}}\frac{\mathrm{d}\phi_r(x)}{\mathrm{d}x}\bigg|_{x=L} \quad (39)$$

and the modal mechanical forcing function is given by equation (27). The discussion regarding the mechanical damping ratio ζ_r is the same as given in section 3.1. Thus, equation (38) is the coupled beam equation in modal coordinates for the bimorph configuration with parallel connection of the piezoceramic layers.

4.2. Coupled electrical circuit equation

It was mentioned in section 2.1 that the piezoceramic layers of the bimorph configuration shown in figure 1(b) are connected in parallel. Since each of the piezoceramic layers can be represented as a current source in parallel with its internal capacitance (section 2.3), figure 4 represents the parallel connection of the identical top and bottom piezoceramic layers of the bimorph configuration shown in figure 1(b).

One can then derive the governing circuit equation based on the Kirchhoff laws as follows:

$$C_{\tilde{\mathrm{p}}}\frac{\mathrm{d}v_{\mathrm{p}}(t)}{\mathrm{d}t} + \frac{v_{\mathrm{p}}(t)}{2R_{\mathrm{l}}} = i_{\tilde{\mathrm{p}}}^{\mathrm{p}}(t) \quad (40)$$

where the internal capacitance and the current source terms for each layer are

$$C_{\tilde{\mathrm{p}}} = \frac{\bar{\varepsilon}_{33}^S bL}{h_{\tilde{\mathrm{p}}}}, \qquad i_{\tilde{\mathrm{p}}}^{\mathrm{p}}(t) = \sum_{r=1}^{\infty}\kappa_r\frac{\mathrm{d}\eta_r^{\mathrm{p}}(t)}{\mathrm{d}t} \quad (41)$$

and the modal coupling term κ_r is given by equation (30). Equation (40) is the electrical circuit equation of the bimorph cantilever for parallel connection of the piezoceramic layers.

4.3. Closed-form voltage response and vibration response expressions

In order to solve for $\eta_r^{\mathrm{p}}(t)$ and $v_{\mathrm{p}}(t)$ in equations (38) and (40), we follow the same procedure given in section 3.3 by assuming the base excitation components in figure 1(b) to be harmonic as $g(t) = Y_0\mathrm{e}^{\mathrm{j}\omega t}$ and $h(t) = \theta_0\mathrm{e}^{\mathrm{j}\omega t}$. For these harmonic base motion inputs of the same frequency, the modal forcing is harmonic as $f_r(t) = F_r\mathrm{e}^{\mathrm{j}\omega t}$ where the amplitude F_r is given by equation (31).

Based on the linear system assumption, the modal mechanical response $\eta_r^{\mathrm{p}}(t)$ and the voltage response $v_{\mathrm{p}}(t)$ are assumed to be harmonic at the frequency of excitation such that $\eta_r^{\mathrm{p}}(t) = H_r^{\mathrm{p}}\mathrm{e}^{\mathrm{j}\omega t}$ and $v_{\mathrm{p}}(t) = V_{\mathrm{p}}\mathrm{e}^{\mathrm{j}\omega t}$, where the amplitudes H_r^{p} and V_{p} are complex valued. Hence, equations (38) and (40) yield the following equations for H_r^{p} and V_{p}:

$$(\omega_r^2 - \omega^2 + \mathrm{j}2\zeta_r\omega_r\omega)H_r^{\mathrm{p}} + \chi_r^p V_{\mathrm{p}} = F_r \quad (42)$$

$$\left(\frac{1}{2R_{\mathrm{l}}} + \mathrm{j}\omega C_{\tilde{\mathrm{p}}}\right)V_{\mathrm{p}} - \mathrm{j}\omega\sum_{r=1}^{\infty}\kappa_r H_r^{\mathrm{p}} = 0 \quad (43)$$

where H_r^{p} and V_{p} can be obtained explicitly. Using the resulting complex voltage amplitude in $v_{\mathrm{p}}(t) = V_{\mathrm{p}}\mathrm{e}^{\mathrm{j}\omega t}$ gives the steady state voltage response as

$$v_{\mathrm{p}}(t) = \frac{\sum_{r=1}^{\infty}\frac{\mathrm{j}\omega\kappa_r F_r}{\omega_r^2-\omega^2+\mathrm{j}2\zeta_r\omega_r\omega}}{\frac{1}{2R_{\mathrm{l}}} + \mathrm{j}\omega C_{\tilde{\mathrm{p}}} + \sum_{r=1}^{\infty}\frac{\mathrm{j}\omega\kappa_r\chi_r^p}{\omega_r^2-\omega^2+\mathrm{j}2\zeta_r\omega_r\omega}}\mathrm{e}^{\mathrm{j}\omega t}. \quad (44)$$

Then the steady state modal mechanical response of the bimorph can be obtained by using V_{p} in equation (42) as

$$\eta_r^{\mathrm{p}}(t) = \left(F_r - \chi_r^p\frac{\sum_{r=1}^{\infty}\frac{\mathrm{j}\omega\kappa_r F_r}{\omega_r^2-\omega^2+\mathrm{j}2\zeta_r\omega_r\omega}}{\frac{1}{2R_{\mathrm{l}}} + \mathrm{j}\omega C_{\tilde{\mathrm{p}}} + \sum_{r=1}^{\infty}\frac{\mathrm{j}\omega\kappa_r\chi_r^p}{\omega_r^2-\omega^2+\mathrm{j}2\zeta_r\omega_r\omega}}\right) \times \frac{\mathrm{e}^{\mathrm{j}\omega t}}{\omega_r^2 - \omega^2 + \mathrm{j}2\zeta_r\omega_r\omega}. \quad (45)$$

The modal mechanical response expression can then be used in equation (11*b*) to obtain the transverse displacement response (relative to the base) at point x on the bimorph:

$$w_{\mathrm{rel}}^{\mathrm{p}}(x,t) = \sum_{r=1}^{\infty}\left[\left(F_r - \chi_r^p\frac{\sum_{r=1}^{\infty}\frac{\mathrm{j}\omega\kappa_r F_r}{\omega_r^2-\omega^2+\mathrm{j}2\zeta_r\omega_r\omega}}{\frac{1}{2R_{\mathrm{l}}} + \mathrm{j}\omega C_{\tilde{\mathrm{p}}} + \sum_{r=1}^{\infty}\frac{\mathrm{j}\omega\kappa_r\chi_r^p}{\omega_r^2-\omega^2+\mathrm{j}2\zeta_r\omega_r\omega}}\right) \times \frac{\phi_r(x)\mathrm{e}^{\mathrm{j}\omega t}}{\omega_r^2 - \omega^2 + \mathrm{j}2\zeta_r\omega_r\omega}\right]. \quad (46)$$

Having obtained the vibration response relative to the moving base, one can easily use superpose the base motion to the relative response to obtain the transverse displacement response at point x relative to the fixed frame as follows:

$$w^{\mathrm{p}}(x,t) = w_{\mathrm{b}}(x,t) + w_{\mathrm{rel}}^{\mathrm{p}}(x,t) \quad (47)$$

where the base displacement $w_{\mathrm{b}}(x,t)$ is given by equation (1).

5. Single-mode electromechanical expressions for modal excitations

The steady state voltage response and vibration response expressions obtained in sections 2 and 3 are valid for harmonic excitations at any arbitrary frequency ω. That is, equations (34) and (36) for series connection of the piezoceramic layers (figure 1(a)) and equations (44) and (46) for parallel connection of the piezoceramic layers (figure 1(b)) are the *multi-mode*

solutions as they include all vibration modes of the bimorph harvester. Hence, these equations can predict the coupled system dynamics not only for resonance excitations but also for excitations at the off-resonance frequencies of the harvester.

In order to obtain the maximum electrical response, it is preferable to excite a given harvester at its fundamental resonance frequency (or at one of the higher resonance frequencies). Most of the studies in the literature have focused on the resonance excitation at the fundamental resonance frequency in order to investigate the maximum performance of the harvester for electrical power generation. Consequently, excitation of a bimorph at or very close to one of its natural frequencies is a very useful problem to investigate through the resulting equations derived in sections 3 and 4. This is the *modal excitation* condition and mathematically it corresponds to $\omega \cong \omega_r$. With this assumption on the excitation frequency, the major contribution in the summation terms of equations (34), (36), (44) and (46) are from the rth vibration mode, which allows drastic simplifications in the coupled voltage and vibration response expressions. In the following, the reduced *single-mode* expressions are given for excitations at or very close to the rth natural frequency, however, it should be noted that the fundamental mode is the main concern in the energy harvesting problem (which corresponds to $r = 1$).

5.1. Series connection of the piezoceramic layers

If the bimorph configuration shown in figure 1(a) is excited at $\omega \cong \omega_r$, the contribution of all the vibration modes other than the rth mode can be ignored in the summation terms. Then, the steady state voltage response given by equation (34) can be reduced to

$$\hat{v}_s(t) = \frac{\mathrm{j}2\omega R_l \kappa_r F_r \mathrm{e}^{\mathrm{j}\omega t}}{(2 + \mathrm{j}\omega R_l C_{\tilde{p}})(\omega_r^2 - \omega^2 + \mathrm{j}2\zeta_r\omega_r\omega) + \mathrm{j}2\omega R_l \kappa_r \chi_r^s} \tag{48}$$

and the transverse displacement relative to the moving base is simply obtained from equation (36) as

$$\hat{w}_{\mathrm{rel}}^{\mathrm{s}}(x,t) = \frac{(2 + \mathrm{j}\omega R_l C_{\tilde{p}}) F_r \phi_r(x) \mathrm{e}^{\mathrm{j}\omega t}}{(2 + \mathrm{j}\omega R_l C_{\tilde{p}})(\omega_r^2 - \omega^2 + \mathrm{j}2\zeta_r\omega_r\omega) + \mathrm{j}2\omega R_l \kappa_r \chi_r^s} \tag{49}$$

where the relevant terms can be found in section 3. Here and below, a hat (ˆ) denotes that the respective term is reduced from the full solution for excitations very close to a natural frequency.

5.2. Parallel connection of the piezoceramic layers

Similarly, if the bimorph configuration displayed in figure 1(b) is excited at $\omega \cong \omega_r$, the steady state voltage response given by equation (44) can be reduced to

$$\hat{v}_p(t) = \frac{\mathrm{j}2\omega R_l \kappa_r F_r \mathrm{e}^{\mathrm{j}\omega t}}{(1 + \mathrm{j}2\omega R_l C_{\tilde{p}})(\omega_r^2 - \omega^2 + \mathrm{j}2\zeta_r\omega_r\omega) + \mathrm{j}2\omega R_l \kappa_r \chi_r^p} \tag{50}$$

and the transverse displacement relative to the base is obtained from equation (46) as

$$\hat{w}_{\mathrm{rel}}^{\mathrm{p}}(x,t) = \frac{(1 + \mathrm{j}2\omega R_l C_{\tilde{p}}) F_r \phi_r(x) \mathrm{e}^{\mathrm{j}\omega t}}{(1 + \mathrm{j}2\omega R_l C_{\tilde{p}})(\omega_r^2 - \omega^2 + \mathrm{j}2\zeta_r\omega_r\omega) + \mathrm{j}2\omega R_l \kappa_r \chi_r^p} \tag{51}$$

where the relevant terms can be found in section 4.

6. Multi-mode and single-mode electromechanical FRFs

In the electromechanical model proposed, the two excitation inputs to the system are the translation of the base in the transverse direction and its small rotation (figures 1(a) and (b)). For these two inputs, the resulting electrical outputs are the voltage response and the vibration response. Therefore, for harmonic base excitations, one can define four electromechanical FRFs between these two outputs and two inputs: voltage output-to-translational base acceleration, voltage output-to-rotational base acceleration, vibration response-to-translational base acceleration and vibration response-to-rotational base acceleration. This section extracts these FRFs from the multi-mode (for arbitrary frequency excitations) and single-mode (for modal excitations) solutions derived in the previous sections.

6.1. Multi-mode electromechanical FRFs

Since the translation and small rotation of the base are given by $g(t) = Y_0 \mathrm{e}^{\mathrm{j}\omega t}$ and $h(t) = \theta_0 \mathrm{e}^{\mathrm{j}\omega t}$, the modal forcing function is in the form of $f_r(t) = F_r \mathrm{e}^{\mathrm{j}\omega t}$ where F_r is given by equation (31). Before identifying the aforementioned FRFs, one should first rearrange the complex modal forcing amplitude given by equation (31) as follows:

$$F_r = -\sigma_r \omega^2 Y_0 - \tau_r \omega^2 \theta_0 \tag{52}$$

where

$$\sigma_r = -m \int_0^L \phi_r(x)\,\mathrm{d}x - M_t \phi_r(L) \tag{53}$$

$$\tau_r = -m \int_0^L x\phi_r(x)\,\mathrm{d}x - M_t L \phi_r(L). \tag{54}$$

6.1.1. Series connection of the piezoceramic layers. The steady state voltage response given by equation (34) can be written in terms of the translational and rotational base accelerations as

$$v_s(t) = \alpha_s(\omega)(-\omega^2 Y_0 \mathrm{e}^{\mathrm{j}\omega t}) + \mu_s(\omega)(-\omega^2 \theta_0 \mathrm{e}^{\mathrm{j}\omega t}) \tag{55}$$

where the FRF that relates the voltage output to translational base acceleration is

$$\alpha_s(\omega) = \frac{\sum_{r=1}^{\infty} \frac{\mathrm{j}\omega\kappa_r\sigma_r}{\omega_r^2 - \omega^2 + \mathrm{j}2\zeta_r\omega_r\omega}}{\frac{1}{R_l} + \mathrm{j}\omega\frac{C_{\tilde{p}}}{2} + \sum_{r=1}^{\infty} \frac{\mathrm{j}\omega\kappa_r\chi_r^s}{\omega_r^2 - \omega^2 + \mathrm{j}2\zeta_r\omega_r\omega}} \tag{56}$$

and the voltage output per rotational base acceleration input can be given by

$$\mu_{\mathrm{s}}(\omega) = \frac{\sum_{r=1}^{\infty} \frac{\mathrm{j}\omega\kappa_r\tau_r}{\omega_r^2-\omega^2+\mathrm{j}2\zeta_r\omega_r\omega}}{\frac{1}{R_{\mathrm{l}}} + \mathrm{j}\omega\frac{C_{\tilde{\mathrm{p}}}}{2} + \sum_{r=1}^{\infty} \frac{\mathrm{j}\omega\kappa_r\chi_r^s}{\omega_r^2-\omega^2+\mathrm{j}2\zeta_r\omega_r\omega}}. \tag{57}$$

Similarly, the steady state vibration response relative to the base of the bimorph given by equation (36) can be expressed as

$$w_{\mathrm{rel}}^{\mathrm{s}}(x,t) = \beta_{\mathrm{s}}(\omega,x)(-\omega^2 Y_0 \mathrm{e}^{\mathrm{j}\omega t}) + \psi_{\mathrm{s}}(\omega,x)(-\omega^2\theta_0\mathrm{e}^{\mathrm{j}\omega t}) \tag{58}$$

where the transverse displacement response-to-translational base acceleration FRF is

$$\beta_{\mathrm{s}}(\omega,x) = \sum_{r=1}^{\infty}\left[\left(\sigma_r - \chi_r^s \frac{\sum_{r=1}^{\infty}\frac{\mathrm{j}\omega\kappa_r\sigma_r}{\omega_r^2-\omega^2+\mathrm{j}2\zeta_r\omega_r\omega}}{\frac{1}{R_{\mathrm{l}}} + \mathrm{j}\omega\frac{C_{\tilde{\mathrm{p}}}}{2} + \sum_{r=1}^{\infty}\frac{\mathrm{j}\omega\kappa_r\chi_r^s}{\omega_r^2-\omega^2+\mathrm{j}2\zeta_r\omega_r\omega}}\right) \times \frac{\phi_r(x)}{\omega_r^2-\omega^2+\mathrm{j}2\zeta_r\omega_r\omega}\right] \tag{59}$$

and the transverse displacement response and rotational base acceleration are related by

$$\psi_{\mathrm{s}}(\omega,x) = \sum_{r=1}^{\infty}\left[\left(\tau_r - \chi_r^s \frac{\sum_{r=1}^{\infty}\frac{\mathrm{j}\omega\kappa_r\tau_r}{\omega_r^2-\omega^2+\mathrm{j}2\zeta_r\omega_r\omega}}{\frac{1}{R_{\mathrm{l}}} + \mathrm{j}\omega\frac{C_{\tilde{\mathrm{p}}}}{2} + \sum_{r=1}^{\infty}\frac{\mathrm{j}\omega\kappa_r\chi_r^s}{\omega_r^2-\omega^2+\mathrm{j}2\zeta_r\omega_r\omega}}\right) \times \frac{\phi_r(x)}{\omega_r^2-\omega^2+\mathrm{j}2\zeta_r\omega_r\omega}\right]. \tag{60}$$

6.1.2. Parallel connection of the piezoceramic layers. It is possible to derive similar FRFs for the parallel connection of the piezoceramic layers. The steady state voltage response given by equation (44) can be rearranged to give

$$v_{\mathrm{p}}(t) = \alpha_{\mathrm{p}}(\omega)\left(-\omega^2 Y_0\mathrm{e}^{\mathrm{j}\omega t}\right) + \mu_{\mathrm{p}}(\omega)(-\omega^2\theta_0\mathrm{e}^{\mathrm{j}\omega t}) \tag{61}$$

where the voltage output-to-translational base acceleration FRF is

$$\alpha_{\mathrm{p}}(\omega) = \frac{\sum_{r=1}^{\infty}\frac{\mathrm{j}\omega\kappa_r\sigma_r}{\omega_r^2-\omega^2+\mathrm{j}2\zeta_r\omega_r\omega}}{\frac{1}{2R_{\mathrm{l}}} + \mathrm{j}\omega C_{\tilde{\mathrm{p}}} + \sum_{r=1}^{\infty}\frac{\mathrm{j}\omega\kappa_r\chi_r^p}{\omega_r^2-\omega^2+\mathrm{j}2\zeta_r\omega_r\omega}} \tag{62}$$

and the voltage output-to-rotational base acceleration FRF can be given by

$$\mu_{\mathrm{p}}(\omega) = \frac{\sum_{r=1}^{\infty}\frac{\mathrm{j}\omega\kappa_r\tau_r}{\omega_r^2-\omega^2+\mathrm{j}2\zeta_r\omega_r\omega}}{\frac{1}{2R_{\mathrm{l}}} + \mathrm{j}\omega C_{\tilde{\mathrm{p}}} + \sum_{r=1}^{\infty}\frac{\mathrm{j}\omega\kappa_r\chi_r^p}{\omega_r^2-\omega^2+\mathrm{j}2\zeta_r\omega_r\omega}}. \tag{63}$$

From equation (46), the steady state vibration response relative to the base of the bimorph can be expressed as

$$w_{\mathrm{rel}}^{\mathrm{p}}(x,t) = \beta_{\mathrm{p}}(\omega,x)(-\omega^2 Y_0\mathrm{e}^{\mathrm{j}\omega t}) + \psi_{\mathrm{p}}(\omega,x)(-\omega^2\theta_0\mathrm{e}^{\mathrm{j}\omega t}) \tag{64}$$

where the transverse displacement response-to-translational base acceleration FRF is

$$\beta_{\mathrm{p}}(\omega,x) = \sum_{r=1}^{\infty}\left[\left(\sigma_r - \chi_r^p \frac{\sum_{r=1}^{\infty}\frac{\mathrm{j}\omega\kappa_r\sigma_r}{\omega_r^2-\omega^2+\mathrm{j}2\zeta_r\omega_r\omega}}{\frac{1}{2R_{\mathrm{l}}} + \mathrm{j}\omega C_{\tilde{\mathrm{p}}} + \sum_{r=1}^{\infty}\frac{\mathrm{j}\omega\kappa_r\chi_r^p}{\omega_r^2-\omega^2+\mathrm{j}2\zeta_r\omega_r\omega}}\right) \times \frac{\phi_r(x)}{\omega_r^2-\omega^2+\mathrm{j}2\zeta_r\omega_r\omega}\right] \tag{65}$$

and the transverse displacement response-to-rotational base acceleration FRF is

$$\psi_{\mathrm{p}}(\omega,x) = \sum_{r=1}^{\infty}\left[\left(\tau_r - \chi_r^p \frac{\sum_{r=1}^{\infty}\frac{\mathrm{j}\omega\kappa_r\tau_r}{\omega_r^2-\omega^2+\mathrm{j}2\zeta_r\omega_r\omega}}{\frac{1}{2R_{\mathrm{l}}} + \mathrm{j}\omega C_{\tilde{\mathrm{p}}} + \sum_{r=1}^{\infty}\frac{\mathrm{j}\omega\kappa_r\chi_r^p}{\omega_r^2-\omega^2+\mathrm{j}2\zeta_r\omega_r\omega}}\right) \times \frac{\phi_r(x)}{\omega_r^2-\omega^2+\mathrm{j}2\zeta_r\omega_r\omega}\right]. \tag{66}$$

6.2. Single-mode electromechanical FRFs

In order to extract the respective FRFs of the single-mode expressions, one should use equations (48)–(51) along with equation (52). In the following, equation (52) is substituted in each of equations (48)–(51) and the relevant FRFs are extracted as done for the multi-mode solution case. Note that, the single-mode electromechanical FRFs given here are strictly valid for modal excitations ($\omega \cong \omega_r$) only.

6.2.1. Series connection of the piezoceramic layers. Equation (48) can be rearranged to give the single-mode steady state voltage response as

$$\hat{v}_{\mathrm{s}}(t) = \hat{\alpha}_{\mathrm{s}}(\omega)(-\omega^2 Y_0\mathrm{e}^{\mathrm{j}\omega t}) + \hat{\mu}_{\mathrm{s}}(\omega)(-\omega^2\theta_0\mathrm{e}^{\mathrm{j}\omega t}) \tag{67}$$

where the single-mode FRF that relates the voltage output to translational base acceleration is

$$\hat{\alpha}_{\mathrm{s}}(\omega) = \frac{\mathrm{j}2\omega R_{\mathrm{l}}\kappa_r\sigma_r}{(2+\mathrm{j}\omega R_{\mathrm{l}}C_{\tilde{\mathrm{p}}})(\omega_r^2-\omega^2+\mathrm{j}2\zeta_r\omega_r\omega) + \mathrm{j}2\omega R_{\mathrm{l}}\kappa_r\chi_r^s} \tag{68}$$

and the single-mode voltage output-to-rotational base acceleration FRF is

$$\hat{\mu}_{\mathrm{s}}(\omega) = \frac{\mathrm{j}2\omega R_{\mathrm{l}}\kappa_r\tau_r}{(2+\mathrm{j}\omega R_{\mathrm{l}}C_{\tilde{\mathrm{p}}})(\omega_r^2-\omega^2+\mathrm{j}2\zeta_r\omega_r\omega) + \mathrm{j}2\omega R_{\mathrm{l}}\kappa_r\chi_r^s}. \tag{69}$$

The single-mode steady state vibration response relative to the base of the bimorph given by equation (49) can be rearranged to give

$$\hat{w}_{\mathrm{rel}}^{\mathrm{s}}(x,t) = \hat{\beta}_{\mathrm{s}}(\omega,x)(-\omega^2 Y_0\mathrm{e}^{\mathrm{j}\omega t}) + \hat{\psi}_{\mathrm{s}}(\omega,x)(-\omega^2\theta_0\mathrm{e}^{\mathrm{j}\omega t}) \tag{70}$$

where the single-mode transverse displacement response-to-translational base acceleration FRF is

$$\hat{\beta}_{\mathrm{s}}(\omega,x) = \frac{(2+\mathrm{j}\omega R_{\mathrm{l}}C_{\tilde{\mathrm{p}}})\sigma_r\phi_r(x)}{(2+\mathrm{j}\omega R_{\mathrm{l}}C_{\tilde{\mathrm{p}}})(\omega_r^2-\omega^2+\mathrm{j}2\zeta_r\omega_r\omega) + \mathrm{j}2\omega R_{\mathrm{l}}\kappa_r\chi_r^s} \tag{71}$$

and the single-mode transverse displacement response-to-rotational base acceleration FRF can be given by

$$\hat{\psi}_{\mathrm{s}}(\omega, x) = \frac{(2 + \mathrm{j}\omega R_{\mathrm{l}} C_{\bar{\mathrm{p}}})\tau_r \phi_r(x)}{(2 + \mathrm{j}\omega R_{\mathrm{l}} C_{\bar{\mathrm{p}}})(\omega_r^2 - \omega^2 + \mathrm{j}2\zeta_r \omega_r \omega) + \mathrm{j}2\omega R_{\mathrm{l}} \kappa_r \chi_r^s}. \quad (72)$$

6.2.2. Parallel connection of the piezoceramic layers. The single-mode steady state voltage response given by equation (50) can be expressed in terms of the translational and rotational base accelerations as

$$\hat{v}_{\mathrm{p}}(t) = \hat{\alpha}_{\mathrm{p}}(\omega)(-\omega^2 Y_0 \mathrm{e}^{\mathrm{j}\omega t}) + \hat{\mu}_{\mathrm{p}}(\omega)(-\omega^2 \theta_0 \mathrm{e}^{\mathrm{j}\omega t}) \quad (73)$$

where the single-mode FRF that relates the voltage output to translational base acceleration is

$$\hat{\alpha}_{\mathrm{p}}(\omega) = \frac{\mathrm{j}2\omega R_{\mathrm{l}} \kappa_r \sigma_r}{(1 + \mathrm{j}2\omega R_{\mathrm{l}} C_{\bar{\mathrm{p}}})(\omega_r^2 - \omega^2 + \mathrm{j}2\zeta_r \omega_r \omega) + \mathrm{j}2\omega R_{\mathrm{l}} \kappa_r \chi_r^p} \quad (74)$$

and the single-mode FRF that relates the voltage output to rotational base acceleration is

$$\hat{\mu}_{\mathrm{p}}(\omega) = \frac{\mathrm{j}2\omega R_{\mathrm{l}} \kappa_r \tau_r}{(1 + \mathrm{j}2\omega R_{\mathrm{l}} C_{\bar{\mathrm{p}}})(\omega_r^2 - \omega^2 + \mathrm{j}2\zeta_r \omega_r \omega) + \mathrm{j}2\omega R_{\mathrm{l}} \kappa_r \chi_r^p}. \quad (75)$$

Similarly, the single-mode steady state vibration response relative to the base of the bimorph given by equation (51) can be rewritten as

$$\hat{w}_{\mathrm{rel}}^{\mathrm{p}}(x, t) = \hat{\beta}_{\mathrm{p}}(\omega, x)(-\omega^2 Y_0 \mathrm{e}^{\mathrm{j}\omega t}) + \hat{\psi}_{\mathrm{p}}(\omega, x)(-\omega^2 \theta_0 \mathrm{e}^{\mathrm{j}\omega t}) \quad (76)$$

where the single-mode transverse displacement response-to-translational base acceleration FRF can be given by

$$\hat{\beta}_{\mathrm{p}}(\omega, x) = \frac{(1 + \mathrm{j}2\omega R_{\mathrm{l}} C_{\bar{\mathrm{p}}})\sigma_r \phi_r(x)}{(1 + \mathrm{j}2\omega R_{\mathrm{l}} C_{\bar{\mathrm{p}}})(\omega_r^2 - \omega^2 + \mathrm{j}2\zeta_r \omega_r \omega) + \mathrm{j}2\omega R_{\mathrm{l}} \kappa_r \chi_r^p} \quad (77)$$

and the single-mode transverse displacement response-to-rotational base acceleration FRF is

$$\hat{\psi}_{\mathrm{p}}(\omega, x) = \frac{(1 + \mathrm{j}2\omega R_{\mathrm{l}} C_{\bar{\mathrm{p}}})\tau_r \phi_r(x)}{(1 + \mathrm{j}2\omega R_{\mathrm{l}} C_{\bar{\mathrm{p}}})(\omega_r^2 - \omega^2 + \mathrm{j}2\zeta_r \omega_r \omega) + \mathrm{j}2\omega R_{\mathrm{l}} \kappa_r \chi_r^p}. \quad (78)$$

7. Experimental validation

This section provides experimental validation of the single-mode analytical relationships. The experimentally measured voltage response-to-base acceleration FRFs and the vibration response-to-base acceleration FRFs are compared with the closed-form FRFs derived in this paper. Variations of the voltage output and the tip velocity response of the bimorph with changing load resistance are also investigated and predicted by using the analytical relations. Since the fundamental vibration mode of the harvester has the highest practical importance for energy harvesting, attention is given to this mode. Variation of the voltage, current and power outputs with load resistance are investigated for excitations at the short circuit and open circuit resonance frequencies of the fundamental mode. Optimum resistive loads of the harvester are identified for excitations at these frequencies.

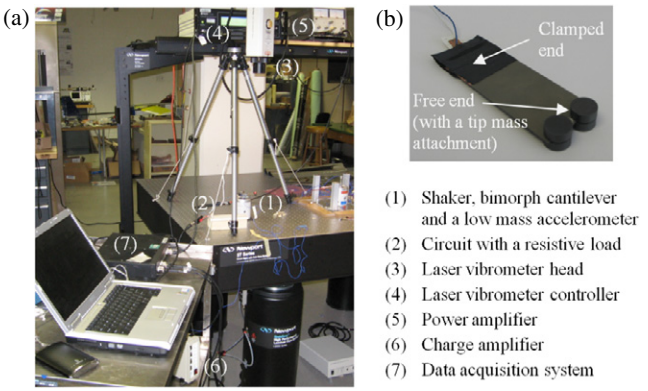

Figure 5. (a) Experimental setup used for validation of the analytical model and the (b) bimorph with a tip mass attachment analyzed in the experiment.

7.1. Experimental setup for a bimorph cantilever with a tip mass

The experimental setup used for measuring the voltage-to-base acceleration and tip velocity-to-base acceleration FRFs of the harvester is shown in figure 5(a). The bimorph analyzed in this experiment is displayed in figure 5(b) and it is manufactured by Piezo Systems, Inc. (T226-A4-503X). The same type of bimorph was recently used by duToit *et al* [33] for the verification of their Rayleigh–Ritz model. Here, we attach a tip mass to the cantilever to make the problem relatively sophisticated in terms of modeling (figure 5(b)). The bimorph consists of two oppositely poled PZT-5A piezoelectric elements bracketing a brass substructure layer. Therefore, the piezoelectric elements are connected in series as schematically given in figure 1(a). The geometric and material properties of the piezoceramic and substructure layers are given in table 1. Note that, in agreement with the formulation given in this paper, the length described by L is the overhang length of the harvester, i.e., it is not the total free length (63.5 mm) of the bimorph as acquired from the manufacturer. In addition, permittivity at constant strain is given in table 1 in terms of the permittivity of free space, $\varepsilon_0 = 8.854$ pF m^{-1} [16].

The bimorph cantilever is excited from its base with a sine sweep generated by an electromagnetic LDS shaker. The base acceleration of the harvester is measured by a low mass accelerometer (PCB U352C22) and the velocity response of the harvester at the free end is measured by a laser vibrometer (Polytec OFV303 laser head, OFV3001 vibrometer). The experimental voltage FRF (in V/g) and tip velocity FRF (in (m/s)/g) obtained for a resistive load of 1 kΩ are shown in figure 6(a). The coherence functions of these measurements

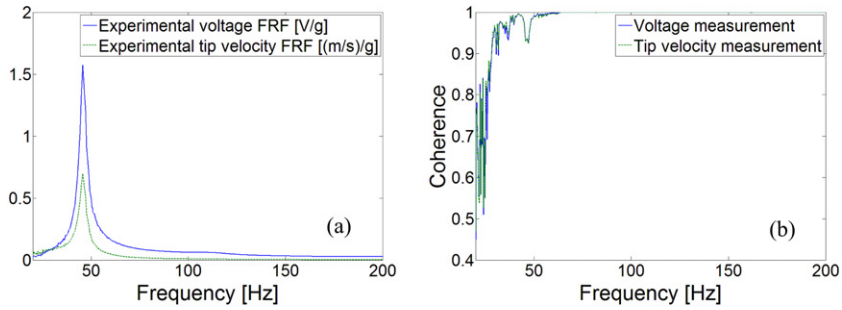

Figure 6. (a) Experimental voltage and tip velocity FRFs of the cantilever and (b) their coherence functions (for a resistive load of 1 kΩ).

Table 1. Geometric and material parameters of the bimorph cantilever used for the experimental validation.

Geometric parameters	Piezo.	Substructure	Material parameters	Piezo (PZT-5A)	Substructure (brass)
Length, L (mm)	50.8	50.8	Mass density, ρ (kg m^{-3})	7800	9000
Width, b (mm)	31.8	31.8	Young's modulus, Y (GPa)	66	105
Thickness, h (mm)	0.26 (each)	0.14	Piezo. constant, d_{31} (pm V^{-1})	−190	—
Tip mass, M_t (kg)	0.012		Permittivity, $\bar{\varepsilon}_{33}^{S}$ (F m^{-1})	$1500\varepsilon_0$	—

are given by figure 6(b). The coherence is considerably low for frequencies less than 30 Hz but it is good around the first resonance frequency (which is approximately 45.6 Hz for a 1 kΩ resistive load).

The single-mode analytical FRFs given by equations (68) and (71) are used in order to validate their accuracy in predicting the experimental observations. Note that the base is not rotating and therefore $\theta_0 = 0$ in equations (67) and (70). The fundamental vibration mode (seen around 45.6 Hz in figure 6(a)) is of practical interest and consequently $r = 1$ is used in equations (68) and (71). It is important to note that the laser vibrometer measures the absolute velocity at the tip of the bimorph in the experiment. However, the tip displacement FRF given by equation (71) for $x = L$ is the displacement of the tip relative to the vibrating base, i.e., it is not relative to the fixed frame. Hence, by considering the absolute displacement given by equation (37), equation (71) must be modified as follows to compare it with the experimental tip velocity measurement:

$$\hat{\beta}_s^{\text{modified}}(\omega, L) = \frac{\frac{d\hat{w}^s(L,t)}{dt}}{-\omega^2 Y_0 e^{j\omega t}} = \frac{\frac{d}{dt}[Y_0 e^{j\omega t} + \hat{w}_{\text{rel}}^s(L,t)]}{-\omega^2 Y_0 e^{j\omega t}}$$
$$= \frac{1}{j\omega} + j\omega\hat{\beta}_s(\omega, L). \tag{79}$$

Thus, the absolute tip velocity FRF given by equation (79) is used in comparisons with the laser vibrometer measurements. Note that, instead of modifying the analytical FRF expression given by equation (71), one could as well process the experimental FRF. However, this option is not preferable because of the possibility of generating noise while post-processing the experimental data. It should also be added that, in the following, the FRFs given by equations (68) and (79) are multiplied by the gravitational acceleration ($g = 9.81$ m s^{-2}) to be in agreement with the experimental measurements (hence the FRFs are given per base acceleration in g). Comparison of the experimental measurements and model predictions are given next.

7.2. Validation of the single-mode expressions and coupled analysis of the harvester

Since the performance of the harvester at resonance is the main concern, accurate identification of mechanical damping ratio is very important. It is a common practice to extract the modal mechanical damping ratio from the first experimental measurement. The uncoupled (but mechanically damped) natural frequency of the harvester can be observed in the experimental FRF by setting $R_l \to 0$ (short circuit conditions), i.e., by using a very low resistive load (since, practically, no wire with zero electrical resistance exists). The measurement provided for 1 kΩ resistive load is close to short circuit conditions for the given harvester and the fundamental natural frequency in short circuit conditions can be extracted from the experimental voltage or tip velocity FRF (figure 6(a)) as 45.6 Hz. By using the numerical data of the bimorph harvester given in table 1, equation (15) predicts the first uncoupled (and mechanically undamped) natural frequency of the harvester analytically as 45.7 Hz. One can then identify the mechanical damping ratio of the first mode by employing the coupled single-mode relations as 2.7%. Hence, this approach allows extracting modal mechanical damping in the presence of a finite resistive load (without forcing the system exactly to be in short circuit conditions). Indeed, if the electromechanical model is *self-consistent*, one must be able to identify the mechanical damping ratio for any value of load resistance. Furthermore, either the voltage FRF or the tip velocity FRF can be used for identifying modal mechanical damping ratio, since the bimorph harvester itself is a *transducer*. In other words, theoretically, the coupled tip velocity information is included in the voltage output information of the harvester, and the voltage and tip motion predictions for the same mechanical damping ratio must be in agreement based on the linear electromechanical system assumption.

The mechanical damping ratio of the first vibration mode is identified (as $\zeta_1 = 0.027$) by using the voltage FRF

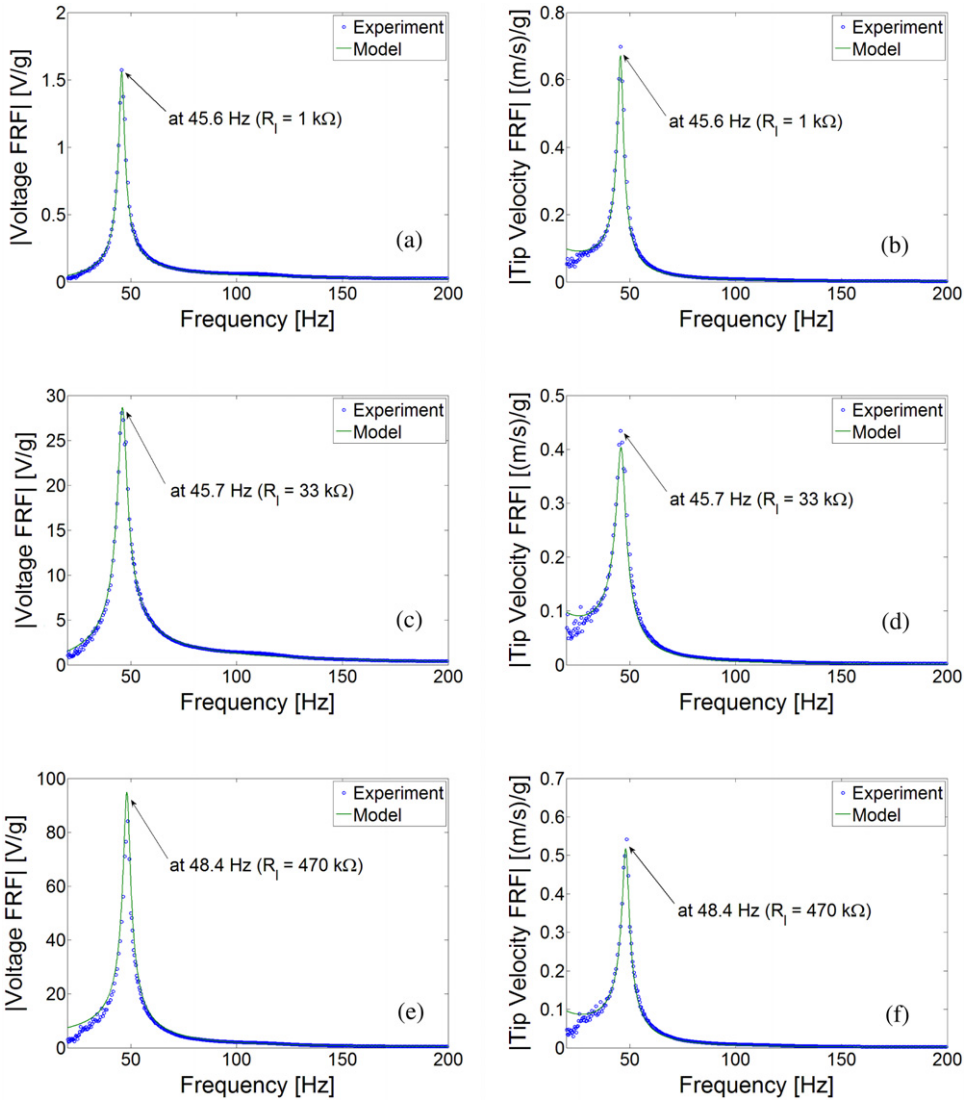

Figure 7. Comparison of the model predictions and experimental measurements; (a) voltage FRF and (b) tip velocity FRF for 1 kΩ, (c) voltage FRF and (d) tip velocity FRF for 33 kΩ, (e) voltage FRF and (f) tip velocity FRF for 470 kΩ.

as shown in figure 7(a) (for 1 kΩ load resistance). For this identified damping ratio, the voltage FRF of the model (obtained from equation (68)) is in perfect agreement with the experimental FRF as shown in figure 7(a). As discussed in the previous paragraph, for the same damping ratio (2.7%), the tip velocity FRF obtained from the model should predict the experimental tip velocity FRF accurately. The tip velocity FRF obtained from equation (79) is plotted with the laser vibrometer measurement in figure 7(b). As can be seen from this figure, the agreement between the theoretical and experimental tip velocity FRFs is very good, which clearly shows the consistency of the electromechanical model proposed here. If the resistive load is replaced by a resistive load of 33 kΩ, the experimental and analytical voltage and tip velocity FRFs given by figures 7(c) and (d) are obtained, respectively. Note that the mechanical damping ratio is kept at 2.7% in the model and the model predicts the coupled structural response successfully for this different resistive load (which is one order of magnitude larger than the previous one). The shift in the resonance frequency for a 33 kΩ resistive load is not very large. However, if the resistive load is increased to 470 kΩ (figures 7(e) and (f)), the resonance frequency moves to 48.4 Hz, which is approximately 2.8 Hz higher than the resonance frequency for 1 kΩ. Note that the system is close to open circuit conditions for the large resistive load of the last case (470 kΩ). The variations in the fundamental mode resonance frequency with changing load resistance as well as the amplitude-wise results in the FRFs are successfully predicted by the analytical model (modal mechanical damping ratio is kept constant at 2.7% in all cases).

From the quantitative point of view, the maximum voltage output increases from 1.57 V/g (at 45.6 Hz) to 84 V/g (at 48.4 Hz) as the resistive load increases from 1 to 470 kΩ. Note that the former case (1 kΩ) is close to short circuit conditions (corresponding to the highest current output) whereas the latter case (470 kΩ) is close to open circuit conditions (yielding the highest voltage output). Therefore, the short circuit and open circuit resonance frequencies for the first mode of this

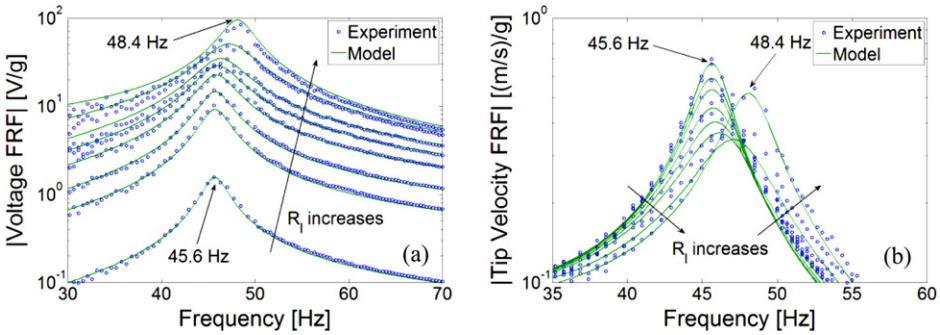

Figure 8. Enlarged views of the (a) voltage FRF and the (b) tip velocity FRF for 8 different values of load resistance (model predictions and the experimental measurements).

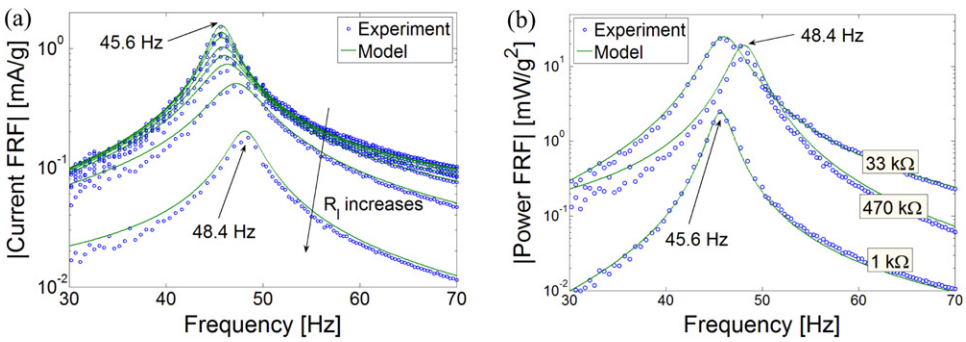

Figure 9. Enlarged views of the (a) current FRF for 8 different values of load resistance and the (b) power FRF 3 different values of load resistance (model predictions and experimental measurements).

harvester are approximately 45.6 Hz and 48.4 Hz, respectively. The analytical model predicts these two frequencies as 45.7 Hz and 48.2 Hz, respectively.

The experimental measurements are repeated for 8 different values of load resistance: 1, 6.7, 11.8, 22, 33, 47, 100 and 470 kΩ. Each of the resistive loads results in a different voltage FRF and a tip velocity FRF. Figures 8(a) and (b), respectively, display enlarged views of the voltage output and tip velocity FRFs around the first vibration mode for these 8 different values of load resistance. The direction of increasing load resistance is depicted with an arrow and it is clear from figure 8(a) that the voltage across the resistive load increases monotonically with increasing load resistance at every excitation frequency. For the extreme values of the load resistance, the frequency of maximum voltage output moves from the short circuit resonance frequency to the open circuit resonance frequency. For a moderate value of load resistance, the frequency of maximum voltage has a value in between these two extreme frequencies (i.e., between 45.6 and 48.4 Hz in this case). The shift in the frequencies of maximum response amplitude is also the case in the tip velocity FRF (figure 8(b)). However, the variation of tip velocity with load resistance is not necessarily monotonic at every frequency. For excitation at 45.6 Hz, the tip motion is suppressed as the resistive load is increased up to a certain value. It is very important to note that this suppression in the motion amplitude is more sophisticated than viscous damping. With increasing load resistance, the motion is *attenuated* at 45.6 Hz whereas it is *amplified* at 48.4 Hz. Hence, if one focuses on the open circuit resonance frequency (48.4 Hz), *both the voltage output and vibration amplitude* at the tip *increases* with increasing load resistance. Therefore, modeling the effect of piezoelectric coupling in the beam equation as viscous damping clearly *fails* in predicting this phenomenon (in addition to the fact that it cannot predict the frequency shift due to changing load resistance). Note that, for 8 different resistive loads, the model predicts the frequency response of the voltage output and tip velocity very successfully.

The electric current FRF exhibits the opposite behavior of the voltage FRF with changing load resistance as shown in figure 9(a) (obtained from $I = V/R_l$). Hence, the electric current decreases monotonically with increasing load resistance at every excitation frequency. Figure 9(b) displays the electrical power FRF for 3 different resistive loads[5]. The trend in the electrical power FRF with changing load resistance is more interesting as it is the multiplication of two FRFs (voltage and current) with the opposite trends. As can be seen in figure 9(b), the electrical power FRFs of different resistive loads intersect each other just like the tip velocity FRF (figure 8(b)). For a given excitation frequency, there exists a certain value of load resistance that gives the maximum electrical power. This value is called the *optimum load resistance* and it can be observed more easily if the frequency

[5] In order to avoid confusion with 8 intersecting curves, the electrical power FRF is given for 3 resistive loads only. Note that the electrical power amplitude is due to $P = |V|^2/R_l$; i.e., it is the peak power. The average power can be obtained from $P_{ave} = |V_{rms}|^2/R_l$, where $V_{rms} = V/\sqrt{2}$ (thus, $P_{ave} = |V|^2/2R_l = P/2$).

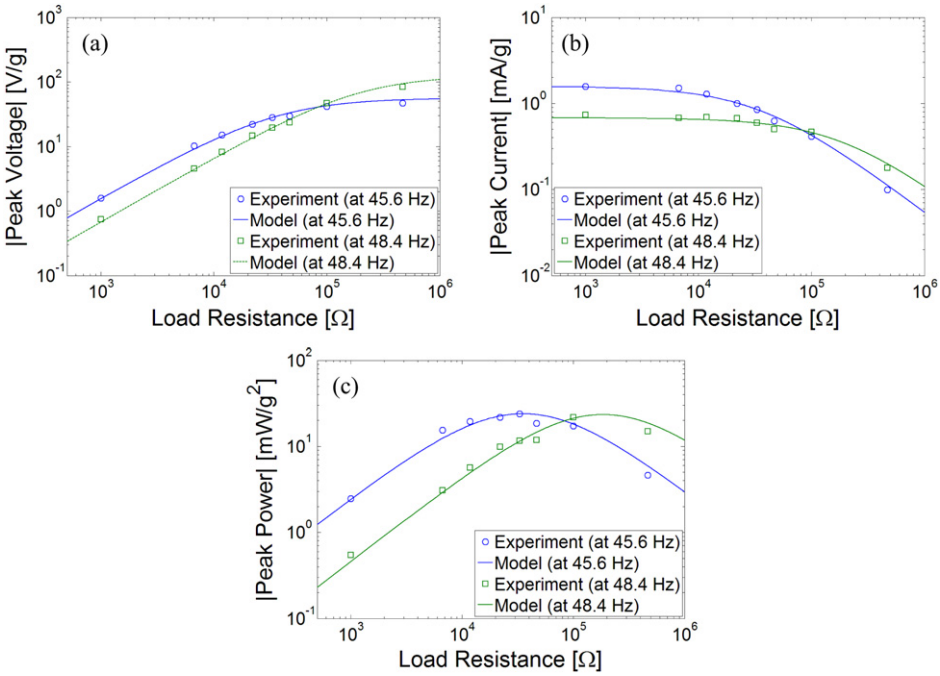

Figure 10. Variations of the (a) peak voltage, (b) peak current and the (b) peak electrical power amplitudes with load resistance for excitations at the short circuit and open circuit resonance frequencies of the first vibration mode.

of interest is kept constant and the power amplitude is plotted against load resistance (which is addressed next).

The short circuit and open circuit resonance frequencies of the first mode are defined for the extreme cases of load resistance (45.6 Hz as $R_l \to 0$ and 48.4 Hz as $R_l \to \infty$) and these frequencies are of practical interest. The variations of the voltage output with changing load resistance for excitations at these two frequencies are shown in figure 10(a). In both cases, voltage increases monotonically with load resistance. The voltage output for excitation at the short circuit resonance frequency is higher when the system is close to short circuit conditions and vice versa. There exists a certain resistive load (83.4 kΩ), for which the voltage response has the same amplitude (40.6 V/g) for excitations at both frequencies. The maximum voltage amplitude in the limit $R_l \to \infty$ is about 54.5 V/g for excitation at 45.6 Hz and it is about 108.8 V/g for excitation at 48.4 Hz. Figure 10(b) shows the variations of the electric current with changing load resistance for excitations at these two frequencies. The trend of the current amplitude with changing load resistance is the opposite of that of the voltage amplitude. That is, the current amplitude decreases monotonically with increasing load resistance. The current output for excitation at the short circuit resonance frequency is higher when the system is close to short circuit conditions and vice versa. Again, for an 83.4 kΩ load resistance, both excitation frequencies yield the same current amplitude (0.49 mA/g). In the limit $R_l \to 0$, the maximum current amplitude is about 1.57 mA/g for excitation at 45.6 Hz and it is about 0.68 mA/g for excitation at 48.4 Hz.

The variation of the electrical power with changing load resistance is given in figure 10(c) for the short circuit and open circuit resonance frequency excitations. As mentioned before, the variation of the electrical power with changing load resistance is not monotonic. These two cases (the short circuit and open circuit resonance frequency excitations) have different optimum resistive loads which yield the maximum electrical power. The optimum load resistance for excitation at 45.6 Hz is about 35 kΩ, yielding a maximum electrical power of about 23.9 mW/g^2 whereas the optimum resistive load for excitation at 48.4 Hz is 186 kΩ, yielding approximately the same power output. As in the case of voltage and current outputs, the electrical power output for excitation at the short circuit resonance frequency is higher when the system is close to short circuit conditions and vice versa. Moreover, for an 83.4 kΩ resistive load, the same electrical power (19.8 mW/g^2) is obtained for excitations at both of these frequencies. The respective trends in the electrical outputs at the short circuit and open circuit resonance frequencies of the first mode are successfully predicted by the single-mode analytical relations derived in this paper.

A useful practice to obtain some additional information regarding the performance of the harvester device implies dividing the electrical power by the volume and by the mass of the harvester. The overhang volume of the bimorph cantilever is 1.07 cm^3 whereas the volume occupied by the tip mass attachment is 2.45 cm^3, yielding a total device volume of about 3.52 cm^3. The overhang mass of the bimorph is 8.6 g and the tip mass is 12 g. Thus, the total mass of the cantilever is about 20.6 g. The electrical power versus load resistance graph given by figure 10(c) can therefore be plotted in the form of *power density* (power per device volume) and *specific power* (power per device mass) graphs. The vertical axis of figure 10(c) must be divided by the device volume to obtain the power density graph and it must be divided by the device mass to obtain the specific power graph. The variations of power density and

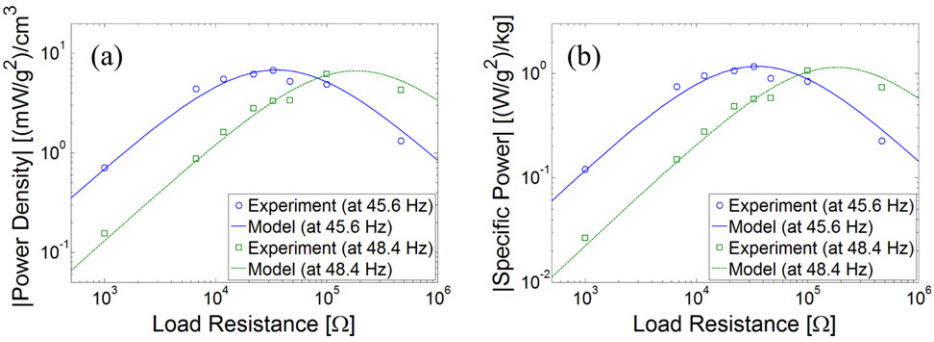

Figure 11. Variations of the (a) power density (power per device volume) and the (b) specific power (power per device mass) amplitudes with load resistance for excitations at the short circuit and open circuit resonance frequencies of the first vibration mode.

specific power with load resistance are given by figures 11(a) and (b), respectively (for the short circuit and open circuit resonance excitations). For instance, for excitation at 45.6 Hz, the maximum power density is about 6.8 (mW/g^2) cm^{-3} and the maximum specific power is about 1.15 (W/g^2) kg^{-1} (for a 35 kΩ resistive load). It is very important to note that the power density and the specific power concepts are *not* complete dimensionless representations. For instance, the same device volume can be occupied by the same amount of material (piezoceramic, substructure and tip mass) for a different aspect ratio of the beam, yielding a larger or smaller electrical power with totally different natural frequencies. Yet, these representations have been found useful for comparison of the harvester devices in the literature.

8. Summary and conclusions

Piezoelectric energy harvesting has been investigated by several researchers for the last five years. Typically, a cantilevered harvester beam with one or two piezoceramic layers is located on a vibrating host structure and the harvester beam generates electrical power due to base excitation. Electromechanical modeling of cantilevered piezoelectric energy harvesters under base excitation has been studied my many authors and the existing models include SDOF approaches, approximate solutions in the sense of Rayleigh–Ritz discretization and analytical solution attempts with certain simplifications. Recently, the authors have presented the closed-form analytical solution for a unimorph cantilever based on the Euler–Bernoulli beam assumptions. In this work, the analytical solution is extended to bimorph configurations with series and parallel connections of piezoceramic layers and experimentally validated.

The base excitation acting on the bimorph cantilever is assumed to be translation in the transverse direction with superimposed small rotation. For series and parallel connections of the piezoceramic layers, the closed-form electromechanical expressions are first obtained for the steady state response to harmonic excitation at arbitrary frequencies. The resulting expressions are then reduced to single-mode expressions by assuming modal excitation (i.e., excitation at or very close to a particular natural frequency), which is the main concern in vibration-based energy harvesting. The single-mode relations given here are easier to use compared to the multi-mode solutions and they are as accurate as the multi-mode solutions for excitations around a natural frequency of interest (which, in general, is the first natural frequency of the harvester). The electromechanical FRFs which relate the voltage output and vibration response of the bimorph to the translational and rotational base acceleration components are extracted both for the multi-mode and single-mode solutions.

In order to validate the model proposed in this paper, an experimental study is presented for a bimorph cantilever with a tip mass attachment. It is shown that the single-mode FRFs obtained from the analytical solution given here can predict the voltage output and the vibration response FRFs of the bimorph very accurately. The base excitation experiments are run for 8 different resistive loads and it is shown that the analytical model can successfully predict the variation in the coupled electrical and mechanical response of the cantilevered bimorph. The outputs of the harvester device (current, voltage and power) are analyzed extensively for the short circuit and open circuit frequency excitations and the accuracy of the single-mode relations is observed in all cases. Since they are based on the distributed parameter solution, the single-mode electromechanical FRFs proposed in this paper here can take the place of the elementary SDOF solutions for modal excitations. Moreover, the single-mode expressions given here are not limited to the fundamental mode and they can be used for any vibration mode as they originate from the distributed parameter solution. The multi-mode closed-form expressions given here can be used if the same harvester is to be excited at different vibration modes or at its off-resonance frequencies due to multi-frequency or varying-frequency inputs.

Acknowledgments

The authors gratefully acknowledge the support of the Air Force Office of Scientific Research MURI under grant number F 9550-06-1-0326 'Energy Harvesting and Storage Systems for Future Air Force Vehicles' monitored by Dr B L Lee. Mr A Erturk acknowledges the support from the 'Liviu Librescu Memorial Scholarship' awarded by the Department of Engineering Science and Mechanics at Virginia Tech. The

authors also thank Mr P Tarazaga for his help in preparing the experimental setup.

References

[1] Williams C B and Yates R B 1996 Analysis of a micro-electric generator for microsystems *Sensors Actuators* A **52** 8–11

[2] Glynne-Jones P, Tudor M J, Beeby S P and White N M 2004 An electromagnetic, vibration-powered generator for intelligent sensor systems *Sensors Actuators* A **110** 344–9

[3] Arnold D 2007 Review of microscale magnetic power generation *IEEE Trans. Magn.* **43** 3940–51

[4] Mitcheson P, Miao P, Start B, Yeatman E, Holmes A and Green T 2004 MEMS electrostatic micro-power generator for low frequency operation *Sensors Actuators* A **115** 523–9

[5] Anton S R and Sodano H A 2007 A review of power harvesting using piezoelectric materials (2003–2006) *Smart Mater. Struct.* **16** R1–21

[6] Priya S 2007 Advances in energy harvesting using low profile piezoelectric transducers *J. Electroceram.* **19** 167–84

[7] Cook-Chennault K A, Thambi N and Sastry A M 2008 Powering MEMS portable devices—a review of non-regenerative and regenerative power supply systems with emphasis on piezoelectric energy harvesting systems *Smart Mater. Struct.* **17** 043001

[8] Beeby S P, Tudor M J and White N M 2006 Energy harvesting vibration sources for microsystems applications *Meas. Sci. Technol.* **13** R175–95

[9] Ottman G K, Hofmann H F, Bhatt A C and Lesieutre G A 2002 Adaptive piezoelectric energy harvesting circuit for wireless remote power supply *IEEE Trans. Power Electron.* **17** 669–76

[10] Guan M J and Liao W H 2007 On the efficiencies of piezoelectric energy harvesting circuits towards storage device voltages *Smart Mater. Struct.* **16** 498–505

[11] Guyomar D, Badel A and Lefeuvre E 2005 Toward energy harvesting using active materials and conversion improvement by nonlinear processing *IEEE Trans. Ultrason. Ferroelectr. Freq. Control* **52** 584–95

[12] Shu Y C and Lien I C 2006 Analysis of power output for piezoelectric energy harvesting systems *Smart Mater. Struct.* **15** 1499–512

[13] Shu Y C, Lien I C and Wu W J 2007 An improved analysis of the SSHI interface in piezoelectric energy harvesting *Smart Mater. Struct.* **16** 2253–64

[14] Roundy S, Wright P and Rabaey J 2003 A study of low level vibrations as a power source for wireless sensor nodes *Comput. Commun.* **26** 1131–44

[15] duToit N E, Wardle B L and Kim S-G 2005 Design considerations for MEMS-scale piezoelectric mechanical vibration energy harvesters *Integr. Ferroelectr.* **71** 121–60

[16] *IEEE Standard on Piezoelectricity* 1987 (New York: IEEE)

[17] Stephen N G 2006 On energy harvesting from ambient vibration *J. Sound Vib.* **293** 409–25

[18] Erturk A and Inman D J 2008 On mechanical modeling of cantilevered piezoelectric vibration energy harvesters *J. Intell. Mater. Syst. Struct.* **19** 1311–25

[19] Hagood N W, Chung W H and Von Flotow A 1990 Modelling of piezoelectric actuator dynamics for active structural control *J. Intell. Mater. Syst. Struct.* **1** 327–54

[20] Crandall S H, Karnopp D C, Kurtz E F Jr and Pridmore-Brown D C 1968 *Dynamics of Mechanical and Electromechanical Systems* (New York: McGraw-Hill)

[21] Sodano H A, Park G and Inman D J 2004 Estimation of electric charge output for piezoelectric energy harvesting *Strain* **40** 49–58

[22] Lu F, Lee H and Lim S 2004 Modeling and analysis of micro piezoelectric power generators for micro-electromechanical-systems applications *Smart Mater. Struct.* **13** 57–63

[23] Chen S-N, Wang G-J and Chien M-C 2006 Analytical modeling of piezoelectric vibration-induced micro power generator *Mechatronics* **16** 379–87

[24] Lin J H, Wu X M, Ren T L and Liu L T 2007 Modeling and simulation of piezoelectric MEMS energy harvesting device *Integr. Ferroelectr.* **95** 128–41

[25] Ajitsaria J, Choe S Y, Shen D and Kim D J 2007 Modeling and analysis of a bimorph piezoelectric cantilever beam for voltage generation *Smart Mater. Struct.* **16** 447–54

[26] Erturk A and Inman D J 2008 Issues in mathematical modeling of piezoelectric energy harvesters *Smart Mater. Struct.* **17** 065016

[27] Erturk A and Inman D J 2008 A distributed parameter electromechanical model for cantilevered piezoelectric energy harvesters *ASME J. Vib. Acoust.* **130** 041002

[28] Elvin N and Elvin A 2008 A general equivalent circuit model for piezoelectric generators *J. Intell. Mater. Syst. Struct.* at press doi:10.1177/1045389X 08089957

[29] Wang Q M and Cross L E 1999 Constitutive equations of symmetrical triple layer piezoelectric benders *IEEE Trans. Ultrason. Ferroelectr. Freq. Control* **46** 1343–51

[30] Clough R W and Penzien J 1975 *Dynamics of Structures* (New York: Wiley)

[31] Banks H T and Inman D J 1991 On damping mechanisms in beams *ASME J. Appl. Mech.* **58** 716–23

[32] Erturk A, Tarazaga P A, Farmer J R and Inman D J 2009 Effect of strain nodes and electrode configuration on piezoelectric energy harvesting from cantilevered beams *ASME J. Vib. Acoust.* at press doi:10.1115/1.2981094

[33] duToit N E and Wardle B L 2007 Experimental verification of models for microfabricated piezoelectric vibration energy harvesters *AIAA J.* **45** 1126–37